An implicit, asymptotic-preserving and energy-charge-conserving method for the Vlasov-Maxwell system near quasineutrality

Chuwen Ma [*†1] and Shi Jin [‡1,2]

[1]School of Mathematical Sciences, Institute of Natural Sciences, Shanghai Jiao Tong University, Shanghai 200240, China.

[2]Ministry of Education, Key Laboratory in Scientific and Engineering Computing, Shanghai Jiao Tong University,Shanghai 200240, China.

April 17, 2023

Abstract

An implicit asymptotic-preserving and energy-charge-conserving (APECC) Particle-In-Cell method is proposed to solve the Vlasov-Maxwell (VM) equations in the quasi-neutral regime. Charge conservation is enforced by particle orbital averaging and fixed sub-time steps. The truncation error depending on the number of sub-time steps is further analyzed. The Crank-Nicolson method is used to exactly conserve the discrete energy. The key step in the asymptotic-preserving iteration for the nonlinear system is based on a decomposition of the current density in the Maxwell model from the Vlasov equation. Moreover, we show that the convergence is independent of the quasi-neutral parameter. Using extensive numerical experiments, we show that the proposed method can achieve asymptotic preservation and energy-charge conservation.

Keywords: Vlasov-Maxwell, Quasi-neutrality, Asymptotic-Preserving, Energy-charge conservation.

1 Introduction

The Vlasov-Maxwell (VM) system is of great importance in the modeling of collisionless magnetized plasmas, with a wide range of applications to fusion devices, high-power microwave generators, and large-scale particle accelerators. The VM system is a coupling of a kinetic equation and a field equations, in which The Vlasov equation describes the motion of microscopic particles, while the electromagnetic field is a solution of the Maxwell equations coupled to the Vlasov equations through the electrical charge and current.

[*]Corresponding author.
[†]chuwenii@sjtu.edu.cn
[‡]shijin-m@sjtu.edu.cn

After scaling, the dimensionless VM system (see Section 2) depends on the scaled Debye length λ. It is the ratio of the physical Debye length λ_D, which is the distance traveled by a particle at thermal velocity in $1/2\pi$ of a plasma cycle, to a spatial scale and is related to the plasma frequency [1, 6]. In the scaled model, the parameter λ appears in the Maxwell-Ampère equation and in Gauss's law. The electric field cannot be obtained explicitly due to the singular nature of the quasi-neutral limit. In addition, the scaled Debye length λ controls the temporal and space frequencies of plasma oscillations and electromagnetic waves, which may become large when $\lambda \to 0$. Therefore, the classical explicit scheme enforces small mesh sizes and time steps to resolve the quasi-neutral parameter. More challenging is the fact that the parameter may vary by orders of magnitude over time and space, which makes traditional domain decomposition methods [18, 19, 22, 35] impossible. A good choice is the Asymptotic-Preserving (AP) scheme, first coined in [29], which switches from a microscopic solver to the macroscopic solver automatically. For more representative AP schemes, we refer to [30]. In literature, a range of AP schemes have been developed for various plasma models in the quasi-neutral regime, including the Euler-Poisson [14], Euler-Maxwell [17], and Vlasov-Poisson systems [16, 25, 26]. For the Vlasov-Maxwell, Degond etc. developed an AP scheme [15] by reformulating the VM system to unify the quasi-neutral model and non-neutral model in a single set of equations.

The VM system itself is energy-charge conserving. But all the aformentioned AP schemes do not conserve the total discrete energy. Numerical noise introduces spurious energies that can erroneously feed plasma instabilities leading to unphysical results. In the study of plasma simulations, it is essential to observe the transformation of energy from one component to another. Most energy-conserving methods are based on implicit methods [7, 9–11, 31, 32]. They relax time-step constrains for stability and have a good property in long time computation.

Clearly, all the fully implicit methods are consistent with both non-neutral and quasi-neutral models. However, a fully implicit discretization requires the solution of a nonlinear system. The convergence of iterative algorithms is severely affected by the small parameter λ. The iterations do not even converge when λ tends to zero. This is because the iterative procedure is usually based on a linearized approach, which leads to the enforcement of some nonlinear constraints depending on λ. There are not many studies that satisfy both energy-charge conservation and asymptotic preservation. Most recently, Ji etc. proposed an Asymptotic-Preserving and energy-conserving (APEC) scheme [28] based on the AP scheme through a Lagrange multiplier to correct the kinetic energy. The goal of this paper is to design, analyze and validate an implicit Asymptotic-Preserving and energy-charge conserving (APECC) Particle-In-Cell method for VM system of plasma physics near quasinutrality. Our AP methodology is partly motivated by the work of Filbet and Jin [21], which is applied to physical problems with stiff source terms that admit stable and unique local equilibrium. However their method was not aimed at nonlinear iterations. The contributions of this work lie in three aspects.

(a) In order to enforce the charge conservation, we modify the particle sub-stepping and orbit-averaging in [8] by using the fixed sub-time steps during one time step. Discrete energy conservation is ensured by implicit methods. We split the current density into two parts —

an implicit part represented by the electric field at the current moment, and an explicit part represented by the results of the previous iteration step. This is the key point for asymptotic preservation.

(b) We derive an error estimate for the particle orbit integrator with respect to the number of sub-time steps. We show that the proposed method is energy and charge conserving, the latter enforcing Gauss's law even when the scaled Debye length λ goes to zero.

(c) We proved the iterative algorithm is well defined as the scaled Debye length λ goes to zero, and the convergence is independent of λ.

We use electrostatic and electromagnetic tests to demonstrate the competitive behavior of the implicit APECC scheme. Compared to the AP scheme, the implicit APECC scheme is able to conserve the discrete energy and charge. In contrast to energy-charge-conserving methods, the proposed method can handle small parameters λ using large time steps and spatial sizes.

The rest of the paper is organized as follows. In Section 2, we introduce the Vlasov-Maxwell system and its quasi-neutral model. In Section 3, we propose the numerical scheme for the VM system by PIC methods and prove the discrete energy and charge conservation. In Section 4, we present the iterative algorithm for the nonlinear system. In Section 5, we prove the asymptotic-preserving properties of the iterative method. Finally, we show the numerical tests in Section 6.

Throughout the paper, vector-valued quantities are denoted by boldface symbols, such as $\boldsymbol{v}_h = (v_{x,h}, v_{y,h}, v_{z,h})$, and matrix-valued quantities by blackboard bold symbols, such as $\mathbb{A} = [a_{ij}] \in \mathbb{R}^{N\times N}$ with $a_{ij} \in \mathbb{R}$. The notation $f \lesssim g$ stands for $f \leq Cg$ where C is independent of the time step $\triangle t$, the spacial size $\triangle x$, the particle mesh h_x, h_v and the scaled Debye length λ. Moreover, $f \eqsim g$ means that $f \lesssim g$ and $g \lesssim f$ hold simultaneously The norm $\|\cdot\|$ used for the discrete vector means $\|\boldsymbol{v}_h\| = \max_h\{|v_{x,h}|, |v_{y,h}|, |v_{z,h}|\}$.

2 The Vlasov-Maxwell system and its quasi-neutral model

For simplicity, we study the evolution of a single species of non-relativistic electrons under a self-consistent electromagnetic field, in which the ion is treated as a homogeneous fixed background with its charge density denoted by ρ_i,

$$\partial_t f + \boldsymbol{v}\cdot\nabla_{\boldsymbol{x}} f + \frac{e}{m}(\boldsymbol{E} + \boldsymbol{v}\times\boldsymbol{B})\cdot\nabla_{\boldsymbol{v}} f = 0, \tag{2.1a}$$

$$\frac{1}{c^2}\partial_t \boldsymbol{E} - \nabla\times\boldsymbol{B} = -\mu_0 \boldsymbol{J}, \tag{2.1b}$$

$$\partial_t \boldsymbol{B} + \nabla\times\boldsymbol{E} = \boldsymbol{0}, \tag{2.1c}$$

$$\nabla\cdot\boldsymbol{E} = \frac{\rho-\rho_i}{\epsilon_0}, \tag{2.1d}$$

$$\nabla\cdot\boldsymbol{B} = 0, \tag{2.1e}$$

where the electron charge densities ρ and the current density $\boldsymbol{J}$ are defined from the distribution function as

$$\rho(\boldsymbol{x},t) = en = e\int_{\Omega_{\boldsymbol{v}}} f(\boldsymbol{x},\boldsymbol{v},t)\,d\boldsymbol{v}, \qquad \boldsymbol{J}(\boldsymbol{x},t) = e\int_{\Omega_{\boldsymbol{v}}} f(\boldsymbol{x},\boldsymbol{v},t)\boldsymbol{v}\,d\boldsymbol{v}. \tag{2.2}$$

Here $f(\boldsymbol{x}, \boldsymbol{v}, t)$ is the particle distribution for electrons in phase space $\Omega_{\boldsymbol{x}} \times \Omega_{\boldsymbol{v}}$, $\boldsymbol{x} \in \Omega_x$ denotes physical position, $\boldsymbol{v} \in \Omega_{\boldsymbol{v}}$ velocity variables. The electric field $\boldsymbol{E}$ and magnetic field $\boldsymbol{B}$ satisfy the Maxwell equations, ϵ_0 and μ_0 are the vacuum permittivity and permeability respectively, c is the speed of light, e, n and m are the electrical charge, density and mass respectively.

It is noted that the Maxwell-Gauss equation (2.1d) and the Maxwell-Thomson equation (2.1e) are the involution of Maxwell's system. Equation (2.1e) is automatically satisfied by taking the divergence of (2.1c). Equation (2.1d) is found from the divergence of the Maxwell-Ampère equation (2.1b) and the continuity equation which is from the integration of the Vlasov equation (2.1a) over Ω_v,

$$\partial_t \rho + \nabla \cdot \boldsymbol{J} = 0. \tag{2.3}$$

2.1 The scaled model and its quasi-neutrality limit

Let x_0, t_0, n_0, v_0, denote the space scale, the time scale, the density and the velocity scale, respectively. The electric field and magnetic field scales are denoted by E_0 and B_0, respectively. The Debye length λ_D is defined by $\lambda_D = \sqrt{m\epsilon_0 v_{th,0}^2/e^2 n_0}$, where $v_{th,0}$ is the electron thermal velocity. Thus the parameter $\lambda = \lambda_D/x_0$ quantifies how close to quasi-neutrality the plasma is. The definition of the quasi-neutral regime from the scaling relations is similar to the most common assumptions of Magneto-Hydro-Dynamic (MHD) model [15]. Under the scaling of the characteristic time, velocity and density by t_0, v_0 and n_0 , length scaled by x_0, characteristic electric, magnetic field and current density by E_0, B_0 and en_0v_0, the distribution function scaled by n_0/v_0, the dimensionless form of the Vlasov equation becomes

$$\partial_t f + \boldsymbol{v} \cdot \nabla_{\boldsymbol{x}} f + (\boldsymbol{E} + \boldsymbol{v} \times \boldsymbol{B}) \cdot \nabla_{\boldsymbol{v}} f = 0. \tag{2.4}$$

The dimensionless Maxwell equation is written as [15]

$$\lambda^2 \partial_t \boldsymbol{E} - \nabla \times \boldsymbol{B} = -\boldsymbol{J}, \qquad \partial_t \boldsymbol{B} + \nabla \times \boldsymbol{E} = 0, \tag{2.5a}$$
$$\lambda^2 \nabla \cdot \boldsymbol{E} = \rho - \rho_i, \qquad \nabla \cdot \boldsymbol{B} = 0, \tag{2.5b}$$

with the density and current density defined by

$$\rho = \int_{\Omega_{\boldsymbol{v}}} f(\boldsymbol{x}, \boldsymbol{v}, t)\, d\boldsymbol{v}, \quad \rho_i = 1, \quad \boldsymbol{J} = \int_{\Omega_{\boldsymbol{v}}} f(\boldsymbol{x}, \boldsymbol{v}, t) \boldsymbol{v}\, d\boldsymbol{v}.$$

Since the rigorous analysis on the convergence of the solutions of the Vlasov-Maxwell system (2.4)–(2.5) to a solution of the quasi-neutral Vlasov-Maxwell system (2.6) when $\lambda \to 0$ is still an open problem, we simply set $\lambda = 0$ in (2.5) to obtain the quasi-neutral model,

$$\partial_t f + \boldsymbol{v} \cdot \nabla_{\boldsymbol{x}} f + (\boldsymbol{E} + \boldsymbol{v} \times \boldsymbol{B}) \cdot \nabla_{\boldsymbol{v}} f = 0, \tag{2.6a}$$
$$\nabla \times \boldsymbol{B} = \boldsymbol{J}, \tag{2.6b}$$
$$\partial_t \boldsymbol{B} + \nabla \times \boldsymbol{E} = 0, \tag{2.6c}$$
$$\rho = 1, \quad \nabla \cdot \boldsymbol{B} = 0. \tag{2.6d}$$

Applying a generalized Ohm law

$$\partial_t \boldsymbol{J} + \nabla \cdot \boldsymbol{S} - \rho \boldsymbol{E} + \boldsymbol{J} \times \boldsymbol{B} = 0,$$

where $\boldsymbol{S} = \int_{\Omega_v} f \boldsymbol{v} \otimes \boldsymbol{v} \, d\boldsymbol{v}$, one gets an equation that equals to (2.6b) [15],

$$\boldsymbol{E} + \nabla \times \nabla \times \boldsymbol{E} = \boldsymbol{J} \times \boldsymbol{B} + \nabla \cdot \boldsymbol{S}, \tag{2.7}$$

provided that $\nabla \times \boldsymbol{B} = \boldsymbol{J}$ at the initial time.

Using particle models, the distribution function f is discretized by a set of particles in phase space,

$$f(\boldsymbol{x}, \boldsymbol{v}, t) \approx \sum_{p=1}^{N_p} \omega_p \delta(\boldsymbol{x} - \boldsymbol{X}_p(t)) \delta(\boldsymbol{v} - \boldsymbol{V}_p(t)), \tag{2.8}$$

where $\omega_p = h_x h_v f(\boldsymbol{X}_p(0), \boldsymbol{V}_p(0), 0)$ is the particle weight, $(\boldsymbol{X}_p(0), \boldsymbol{V}_p(0))$ denotes the cell center of the phase-space grid, h_x and h_v are the particle mesh spacing in physical space and velocity space, respectively, and N_p is the number of particles. Each particle follows the trajectory of the flow,

$$\frac{\mathrm{d}\boldsymbol{X}_p}{\mathrm{d}t} = \boldsymbol{V}_p, \qquad \frac{\mathrm{d}\boldsymbol{V}_p}{\mathrm{d}t} = \boldsymbol{E}(\boldsymbol{X}_p) + \boldsymbol{V}_p \times \boldsymbol{B}(\boldsymbol{X}_p), \tag{2.9}$$

where $\boldsymbol{E}$ and $\boldsymbol{B}$ are the induced fields from the Maxwell equations (2.5). Therefore, the charge density and current density are from the particles,

$$\rho = \sum_{p=1}^{N_p} \omega_p \delta(\boldsymbol{x} - \boldsymbol{X}_p(t)), \qquad \boldsymbol{J} = \sum_{p=1}^{N_p} \omega_p \boldsymbol{V}_p \delta(\boldsymbol{x} - \boldsymbol{X}_p(t)). \tag{2.10}$$

Remark 2.1. The particle model is an approximation to the original one and the number of particles determines the accuracy of the approximation. For interesting previous works on the convergence of the particle method, we refer to [2, 12, 13, 23, 24, 38].

3 Numerical scheme

In this section, we present a discretization scheme for the Vlasov-Maxwell system. We use a Crank-Nicolson (CN) mover to push the particles and advance Maxwell's equations. In addition, we employ the Yee finite difference for the field approximation.

To ensure discrete charge conservation, previous studies [7, 9] have argued that automatic charge conservation is enforced by stopping particles at the cell surface. In their recent research [8], particle sub-stepping and orbit-averaging were used to allow for a large time step. We follow the idea but use a fixed sub-time step during each time step.

Let $t^m = m\triangle t$, $m = 0, 1, \cdots, M$, be a uniform partition of the interval $[0, T]$ and $\triangle t = T/M$. Assume the acceleration is independent of time during each time step, and the trajectory is a straight line during each sub time step $\tau = \triangle t/(N_s + 1)$, where N_s is an integer. The particle position and velocity at time $t^{m,s}$ are denoted by $(\boldsymbol{X}_p^{m_s}, \boldsymbol{V}_p^{m_s})$, where $t^{m,s} = t^m + s\tau$ and $(\boldsymbol{X}_p^{m_0}, \boldsymbol{V}_p^{m_0}) = (\boldsymbol{X}_p^m, \boldsymbol{V}_p^m)$, $(\boldsymbol{X}_p^{m_{N_s+1}}, \boldsymbol{V}_p^{m_{N_s+1}}) = (\boldsymbol{X}_p^{m+1}, \boldsymbol{V}_p^{m+1})$. For $s = 0, \cdots, N_s$, the movement of each particle from time $t^{m,s}$ to $t^{m,s+1}$ is

$$\begin{aligned}
\boldsymbol{X}_p^{m_{s+1}} - \boldsymbol{X}_p^{m_s} &= \frac{\tau}{2}(\boldsymbol{V}_p^{m_{s+1}} + \boldsymbol{V}_p^{m_s}), \\
\boldsymbol{V}_p^{m_{s+1}} - \boldsymbol{V}_p^{m_s} &= \sum_{l=0}^{L_p^{m_s}} \frac{\tau_{pl}^{m_s}}{2} \Big(\boldsymbol{E}_I^{m+1}(\boldsymbol{X}_p^{m_{s,l+\frac{1}{2}}}) + \boldsymbol{E}_I^m(\boldsymbol{X}_p^{m_{s,l+\frac{1}{2}}}) + (\boldsymbol{V}_p^{m_{s+1}} + \boldsymbol{V}_p^{m_s}) \times \boldsymbol{B}_I^m(\boldsymbol{X}_p^{m_{s,l+\frac{1}{2}}}) \Big),
\end{aligned} \tag{3.1}$$

where $\boldsymbol{X}_p^{m_s,l+1/2} = \big(\boldsymbol{X}_p^{m_s,l+1} + \boldsymbol{X}_p^{m_s,l}\big)/2$, the discrete electric field $\boldsymbol{E}_h^{m+1}$, $\boldsymbol{E}_h^{m}$ and magnetic field $\boldsymbol{B}_h^{m}$ are induced from discrete Maxwell equations. The particle $\boldsymbol{X}_p^{m_s,l}$ stops at cell surfaces for $l = 1, \cdots, L_p^{m_s}$, and $L_p^{m_s}$ is determined by the number of cell-crossing. The sub time step $\tau_{pl}^{m_s}$ of τ from $\boldsymbol{X}_p^{m_s,l}$ to $\boldsymbol{X}_p^{m_s,l+1}$ is defined by $\tau_{pl}^{m_s} = \tau \left|\boldsymbol{X}_p^{m_s,l+1} - \boldsymbol{X}_p^{m_s,l}\right| / \left|\boldsymbol{X}_p^{m_s+1} - \boldsymbol{X}_p^{m_s}\right|$, and satisfies $\tau = \sum_{l=0}^{L_p^{m_s}} \tau_{pl}^{m_s}$. The interpolation functions $\boldsymbol{E}_I^{m+1}(\boldsymbol{X}_p^{m_s,l+1/2})$ and $\boldsymbol{B}_I^{m}(\boldsymbol{X}_p^{m_s,l+\frac{1}{2}})$ are defined by

$$\boldsymbol{E}_I^{m+1}(\boldsymbol{X}_p^{m_s,l+1/2}) = \sum_h \boldsymbol{E}_h^{m+1} \cdot \boldsymbol{S}^{m_s,l+1/2}(\boldsymbol{x}_h - \boldsymbol{X}_p), \quad \boldsymbol{B}_I^{m}(\boldsymbol{X}_p^{m_s,l+1/2}) = \sum_h \boldsymbol{B}_h^{m} \cdot \boldsymbol{S}^{m_s,l+1/2}(\boldsymbol{x}_h - \boldsymbol{X}_p). \tag{3.2}$$

Here $\boldsymbol{x}_h$ is the grid location, $\boldsymbol{X}_p$ is the particle position depending on $\boldsymbol{X}_p^{m_s,l}$ and $\boldsymbol{X}_p^{m_s,l+1}$, and $\boldsymbol{S}^{m_s,l+1/2}$ is a special shape function proposed in [8] to ensure energy, defined by

$$\begin{aligned}\boldsymbol{S}^{m_s,l+1/2}(\boldsymbol{x}_h - \boldsymbol{X}_p) = {}& \boldsymbol{i} \otimes \boldsymbol{i}\, S_1(x_{i+1/2} - X_p^{m_s,l+1/2}) S_{22,jk}^{m_s,l+1/2} + \boldsymbol{j} \otimes \boldsymbol{j}\, S_1(y_{j+1/2} - Y_p^{m_s,l+1/2}) S_{22,ik}^{m_s,l+1/2} \\ & + \boldsymbol{k} \otimes \boldsymbol{k}\, S_1(z_{k+1/2} - Z_p^{m_s,l+1/2}) S_{22,ij}^{m_s,l+1/2},\end{aligned} \tag{3.3}$$

where $\boldsymbol{i}$, $\boldsymbol{j}$ and $\boldsymbol{k}$ are unit vectors in the x, y and z directions, respectively, $S_1(x_{i+1/2} - X_p^{m_s,l+1/2})$ is the linear B-spline shape function, and

$$\begin{aligned}S_{22,jk}^{m_s+1/2} = {}& \frac{1}{3}\Big(S_2(y_j - Y_p^{m_s,l+1}) S_2(z_k - Z_p^{m_s,l+1}) + S_2(y_j - Y_p^{m_s,l}) S_2(z_k - Z_p^{m_s,l+1})/2\Big) \\ & + \frac{1}{3}\Big(S_2(y_j - Y_p^{m_s,l}) S_2(z_k - Z_p^{m_s,l}) + S_2(y_j - Y_p^{m_s,l+1}) S_2(z_k - Z_p^{m_s,l})/2\Big),\end{aligned} \tag{3.4}$$

with $S_2(z_k - Z_p^{m_s,l+1})$ the second-order B-spline function.

The Yee algorithm [37] centers its $\boldsymbol{E}_h$ and $\boldsymbol{B}_h$ components at the edges and surfaces of the cell, respectively. Thus each component of $\boldsymbol{E}_h$ is surrounded by four cyclic components of $\boldsymbol{B}_h$, and so is each component of $\boldsymbol{B}_h$. The discretization scheme for the Maxwell system is written as

$$\frac{\lambda^2}{\triangle t}(\boldsymbol{E}_h^{m+1} - \boldsymbol{E}_h^{m}) - \nabla_h \times \frac{\boldsymbol{B}_h^{m+1} + \boldsymbol{B}_h^{m}}{2} = -\boldsymbol{J}_h^{m+1/2}, \tag{3.5}$$

$$\frac{1}{\triangle t}(\boldsymbol{B}_h^{m+1} - \boldsymbol{B}_h^{m}) + \nabla_h \times \frac{\boldsymbol{E}_h^{m+1} + \boldsymbol{E}_h^{m}}{2} = 0, \tag{3.6}$$

where the current density is defined by

$$\boldsymbol{J}_h^{m+1/2} = \frac{1}{V_o \triangle t} \sum_{p=1}^{N_p} \sum_{s=0}^{N_s} \omega_p \boldsymbol{V}_p^{m_s+1/2} \cdot \sum_{l=0}^{L_p^{m_s}} \boldsymbol{S}^{m_s,l+1/2}(\boldsymbol{x}_h - \boldsymbol{X}_p) \tau_{pl}^{m_s}. \tag{3.7}$$

Here $\boldsymbol{V}_p^{m_s+1/2} = (\boldsymbol{V}_p^{m_s+1} + \boldsymbol{V}_p^{m_s})/2$, and $V_o = \triangle x \triangle y \triangle z$ is the cell volume, $\triangle x$, $\triangle y$ and $\triangle z$ are mesh sizes along the x, y and z directions, respectively. The finite-difference expressions for the space derivatives used in the curl operators are central difference. The central-difference operations are also used in divergence operators. Naturally, it yields

$$\nabla_h \cdot (\nabla_h \times \boldsymbol{E}_h) = 0, \quad \nabla_h \cdot (\boldsymbol{E}_h \times \boldsymbol{B}_h) = \boldsymbol{B}_h \cdot (\nabla_h \times \boldsymbol{E}_h) - \boldsymbol{E}_h \cdot (\nabla_h \times \boldsymbol{B}_h). \tag{3.8}$$

Taking the discrete divergence of (3.6), we obtain the solenoidal property of the discrete magnetic field i.e. $\nabla_h \cdot \boldsymbol{B}_h^{m+1} = 0$ for any $m \geq 0$, as long as the initial magnetic field is divergence free. It is noted that

$$\frac{\lambda^2}{\triangle t} \nabla_h \cdot (\boldsymbol{E}_h^{m+1} - \boldsymbol{E}_h^{m}) = -\nabla_h \cdot \boldsymbol{J}_h^{m+1/2}. \tag{3.9}$$

Gauss's law is enforced by exact charge conservation,

$$\frac{\rho_h^{m+1}-\rho_h^m}{\triangle t}+\nabla_h\cdot\boldsymbol{J}_h^{m+1/2}=0. \tag{3.10}$$

3.1 Energy conservation

In this section, we will prove that the numerical scheme of (3.1)–(3.6) preserves the energy conservation law. For easy notations, let $\boldsymbol{E}_h^{m+1/2}=(\boldsymbol{E}_h^{m+1}+\boldsymbol{E}_h^m)/2$, $\boldsymbol{B}_h^{m+1/2}=(\boldsymbol{B}_h^{m+1}+\boldsymbol{B}_h^m)/2$, and define the electrical energy, the magnetic energy, the kinetic energy as:

$$W_E^m=\frac{\lambda^2}{2}\sum_h(\boldsymbol{E}_h^m)^2V_o,\quad W_B^m=\frac{1}{2}\sum_h(\boldsymbol{B}_h^m)^2V_o,\quad W_V^m=\frac{1}{2}\sum_p\omega_p(\boldsymbol{V}_p^m)^2. \tag{3.11}$$

Since the current density and electromagnetic fields use the same shape functions, we obtain

$$\begin{aligned}\sum_h\boldsymbol{J}_h^{m+1/2}\cdot\boldsymbol{E}_h^{m+1/2}&=\frac{1}{V_o\triangle t}\sum_{p=1}^{N_p}\sum_{s=0}^{N_s}\omega_p\boldsymbol{V}_p^{m_s+1/2}\cdot\sum_{l=0}^{L_p^{m_s}}\sum_h\boldsymbol{S}^{m_s,l+1/2}(\boldsymbol{x}_h-\boldsymbol{X}_p)\boldsymbol{E}_h^{m+1/2}\tau_{pl}^{m_s}\\&=\frac{1}{V_o\triangle t}\sum_{p=1}^{N_p}\sum_{s=0}^{N_s}\omega_p\boldsymbol{V}_p^{m_s+1/2}\cdot\sum_{l=0}^{L_p^{m_s}}\boldsymbol{E}_I^{m+1/2}(\boldsymbol{X}_p^{m_s,l+1/2})\tau_{pl}^{m_s}.\end{aligned}$$

From (3.1) and the equality $\boldsymbol{V}_p^{m_s+1/2}\cdot(\boldsymbol{V}_p^{m_s+1/2}\times\boldsymbol{B}_I^m(X_p^{m_s,l+1/2}))=0$, we have

$$V_o\triangle t\sum_h\boldsymbol{J}_h^{m+1/2}\cdot\boldsymbol{E}_h^{m+1/2}=\sum_{p=1}^{N_p}\sum_{s=0}^{N_s}\omega_p\boldsymbol{V}_p^{m_s+1/2}\cdot(\boldsymbol{V}_p^{m_s+1}-\boldsymbol{V}_p^{m_s})=W_V^{m+1}-W_V^m. \tag{3.12}$$

Multiplying (3.5) by $\boldsymbol{E}_h^{m+1/2}V_o$ and summing over the term h, it yields

$$\left(W_E^{m+1}-W_E^m\right)-\sum_h(\nabla_h\times\boldsymbol{B}_h^{m+1/2})\cdot\boldsymbol{E}_h^{m+1/2}V_o\triangle t=-\sum_h\boldsymbol{J}_h^{m+1/2}\cdot\boldsymbol{E}_h^{m+1/2}V_o\triangle t. \tag{3.13}$$

Multiplying (3.6) by $\boldsymbol{B}_h^{m+1/2}V_o$, summing over h and using (3.8) and periodic boundary condition yield

$$\left(W_B^{m+1}-W_B^m\right)+\sum_h(\nabla_h\times\boldsymbol{B}_h^{m+1/2})\cdot\boldsymbol{E}_h^{m+1/2}V_o\triangle t=0. \tag{3.14}$$

By summing up equations (3.12), (3.13) and (3.14) together, we get

$$W_E^{m+1}+W_B^{m+1}+W_V^{m+1}=W_E^m+W_B^m+W_V^m.$$

3.2 Charge conservation

In order to obtain that the charge conservation is ensured, we employ second-order B-splines for the charge density of the p-th particle,

$$\rho_p^m=\omega_pS_2(x_i-X_p^m)S_2(y_j-Y_p^m)S_2(z_k-Z_p^m)/V_o, \tag{3.15}$$

where (i,j,k) is the mesh index. The current density of each particle during the sub time step $\tau_{pl}^{m_s}$ is defined by

$$\boldsymbol{J}_p^{m_s,l+1/2}=\omega_p\boldsymbol{V}_p^{m_s+1/2}\cdot\boldsymbol{S}^{m_s,l+1/2}(\boldsymbol{x}_h-\boldsymbol{X}_p)/V_o. \tag{3.16}$$

Since $\boldsymbol{X}_p^{m_s,l}$, $l = 1, \cdots, L_p^{m_s}$ stops at the cell surface, along each direction, Taylor's expansion shows [7, 9]

$$\frac{S_2(x_i - X_p^{m_s,l+1}) - S_2(x_i - X_p^{m_s,l})}{\tau_{pl}^{m_s}} + V_{x,p}^{m_s+1/2}\frac{S_1(x_{i+1/2} - X_p^{m_s,l+1/2}) - S_1(x_{i-1/2} - X_p^{m_s,l+1/2})}{\triangle x} = 0, \tag{3.17}$$

where $V_{x,p}^{m_s+1/2}$ is the first component of $\boldsymbol{V}_p^{m_s+1/2}$. Due to the definition of $\boldsymbol{J}_p^{m_s,l+1/2}$ and ρ_p^m, taking the sum of l and s, one gets

$$\frac{\rho_p^{m+1} - \rho_p^m}{\triangle t} + \nabla_h \cdot \sum_{s=0}^{N_s}\sum_{l=0}^{L_p^{m_s}} \tau_{pl}^{m_s}\boldsymbol{J}_p^{m_s,l+1/2}/\triangle t = 0. \tag{3.18}$$

Since the discrete charge and current density are defined by

$$\rho_h^m = \sum_{p=1}^{N_p}\rho_p^m, \qquad \boldsymbol{J}_h^{m+1/2} = \sum_{p=1}^{N_p}\sum_{s=0}^{N_s}\sum_{l=0}^{L_p^{m_s}}\boldsymbol{J}_p^{m_s,l+1/2}\tau_{pl}^{m_s}/\triangle t. \tag{3.19}$$

It is easy to see that the discrete charge conservation is enforced.

3.3 Sub-step of pushing particles

It is noted that using $\boldsymbol{B}_I^{m+\frac{1}{2}}(\boldsymbol{X}_p^{m_s,l+\frac{1}{2}})$ in (3.1) leads to a Crank-Nicolson scheme for pushing particles, and it still conserves the energy because the magnetic field does no work on a charged particle. In addition, charge conservation is still enforced since it does not affect the definition of current and charge density. In this section, we show the dependence of the local truncation error of the particle movement on the number of sub-steps N_s. We rewrite (3.1) with a CN mover as

$$\begin{aligned}\boldsymbol{X}_p^{m_s+1} - \boldsymbol{X}_p^{m_s} &= \tau(\boldsymbol{V}_p^{m_s+1} + \boldsymbol{V}_p^{m_s})/2,\\ \boldsymbol{V}_p^{m_s+1} - \boldsymbol{V}_p^{m_s} &= \sum_{l=0}^{L_p^{m_s}}\tau_{pl}^{m_s}\big(\boldsymbol{a}^{m+1}(\boldsymbol{X}_p^{m_s,l+1/2}) + \boldsymbol{a}^m(\boldsymbol{X}_p^{m_s,l+1/2})\big)/2.\end{aligned} \tag{3.20}$$

Here $\boldsymbol{a}^{m+1}$ is the acceleration at time t^{m+1}. A Simple calculation yields

$$\boldsymbol{X}_p^{m+1} = \boldsymbol{X}_p^m + \boldsymbol{V}_p^m\triangle t + \frac{\tau}{4}\sum_{s=0}^{N_s}\sum_{l=0}^{L_p^{m_s}}(2N_s - 2s + 1)\tau_{pl}^{m_s}\big(\boldsymbol{a}^{m+1}(\boldsymbol{X}_p^{m_s,l+1/2}) + \boldsymbol{a}^m(\boldsymbol{X}_p^{m_s,l+1/2})\big). \tag{3.21}$$

Taylor's expansion shows that

$$\begin{aligned}\boldsymbol{X}_p^{m+1} =& \boldsymbol{X}_p^m + \boldsymbol{V}_p^m\triangle t + \frac{\triangle t^2}{2}\boldsymbol{a}^m(\boldsymbol{X}_p^m)\\ &+ \frac{\triangle t^3}{4}\partial_t\boldsymbol{a}^m(\boldsymbol{X}_p^m) + \frac{(2N_s^2 + 4N_s + 3)\triangle t^3}{12(N_s+1)^2}\partial_x\boldsymbol{a}^m(\boldsymbol{X}_p^m)\boldsymbol{V}_p^m + O(\triangle t^4).\end{aligned} \tag{3.22}$$

The exact solution has the following expansion:

$$\boldsymbol{X}_p^{m+1} = \boldsymbol{X}_p^m + \boldsymbol{V}_p^m\triangle t + \frac{\triangle t^2}{2}\boldsymbol{a}^m(\boldsymbol{X}_p^m) + \frac{\triangle t^3}{6}\partial_t\boldsymbol{a}^m(\boldsymbol{X}_p^m) + \frac{\triangle t^3}{6}\partial_x\boldsymbol{a}^m(\boldsymbol{X}_p^m)\boldsymbol{V}_p^m + O(\triangle t^4). \tag{3.23}$$

Comparing (3.22) and (3.23), the leading truncation error is estimated by

$$\mathrm{Err} = \frac{\triangle t^3}{12}\partial_t\boldsymbol{a}^m(\boldsymbol{X}_p^m) + \frac{\triangle t^3}{12(N_s+1)^2}\partial_x\boldsymbol{a}^m(\boldsymbol{X}_p^m)\boldsymbol{V}_p^m. \tag{3.24}$$

It can be seen from (3.24) that the truncation error consists of two parts – the temporal approximation and the spatial approximation, only the latter is affected by the number of sub-steps N_s. Therefore, it is not economical to increase N_s to improve the accuracy of the calculation, since large N_s implies large computation. However, large N_s leads to quick nonlinear iteration, noting that (3.20) requires a nonlinear solver. In the numerical test, we usually choose $N_s = 0$ or $N_s = 1$, which results in fast convergence of the nonlinear solver for (3.20) and good accuracy of the particle orbits.

4 Iterative algorithm

Since the numerical scheme is a nonlinear system, in this section, we present a fixed point iteration to solve the numerical scheme.

4.1 Reference implicit iterative algorithm

The reference iterative algorithm for the nonlinear system (3.1) –(3.6) is denoted by the implicit energy-charge conserving (ECC) scheme, which is listed in Algorithm 1. Compared to the

Algorithm 1 An implicit ECC algorithm for the Vlasov-Maxwell equations

1. Given $\boldsymbol{E}_h^m$, $\boldsymbol{B}_h^m$, $\boldsymbol{X}_p^m$, $\boldsymbol{V}_p^m$, start with $\boldsymbol{E}_h^{m+1,k=1} = \boldsymbol{E}_h^m$ (k is the iteration index).

2. Start from $\boldsymbol{X}_p^{m_0} = \boldsymbol{X}_p^m$, $\boldsymbol{V}_p^{m_0} = \boldsymbol{V}_p^m$. For $s = 0, 1, \cdots, N_s$, update $\boldsymbol{X}_p^{m_{s+1},k}$ and $\boldsymbol{V}_p^{m_{s+1},k}$ by
$$\begin{aligned}\boldsymbol{X}_p^{m_{s+1},k} - \boldsymbol{X}_p^{m_s,k} =& \frac{\tau}{2}(\boldsymbol{V}_p^{m_{s+1},k} + \boldsymbol{V}_p^{m_s,k}),\\ \boldsymbol{V}_p^{m_{s+1},k} - \boldsymbol{V}_p^{m_s,k} =& \frac{1}{2}\sum_{l=0}^{L_p^{m_s,k}} \tau_{pj}^{m_s,k}\Big(\boldsymbol{E}_I^{m+1,k}(\boldsymbol{X}_p^{m_{s,l+\frac{1}{2}},k}) + \boldsymbol{E}_I^m(\boldsymbol{X}_p^{m_{s,l+\frac{1}{2}},k})\\ &+ (\boldsymbol{V}_p^{m_{s+1},k} + \boldsymbol{V}_p^{m_s,k}) \times \boldsymbol{B}_I^m(\boldsymbol{X}_p^{m_{s,l+\frac{1}{2}},k})\Big).\end{aligned} \tag{4.1}$$

3. Compute the current density
$$\boldsymbol{J}_h^{m+1/2,k} = \frac{1}{2\triangle t V_o}\sum_{p=1}^{N_p}\omega_p\sum_{s=0}^{N_s}(\boldsymbol{V}_p^{m_s,k} + \boldsymbol{V}_p^{m_{s+1},k}) \cdot \sum_{l=0}^{L_p^{m_s,k}} \boldsymbol{S}^{m_{s,l+1/2},k}(\boldsymbol{x}_h - \boldsymbol{X}_p)\tau_{pl}^{m_s,k}. \tag{4.2}$$

4. The electric filed $\boldsymbol{E}_h^{m+1,k+1}$ and magnetic field $\boldsymbol{B}_h^{m+1,k+1}$ are obtained by solving
$$\begin{aligned}\frac{\lambda^2}{\triangle t}\boldsymbol{E}_h^{m+1,k+1} - \frac{1}{2}\nabla_h \times (\boldsymbol{B}_h^{m+1,k+1} + \boldsymbol{B}_h^m) = \frac{\lambda^2}{\triangle t}\boldsymbol{E}_h^m - \boldsymbol{J}_h^{m+1/2,k},\\ \frac{1}{\triangle t}\boldsymbol{B}_h^{m+1,k+1} + \frac{1}{2}\nabla_h \times (\boldsymbol{E}_h^{m+1,k+1} + \boldsymbol{E}_h^m) = \frac{1}{\triangle t}\boldsymbol{B}_h^m.\end{aligned} \tag{4.3}$$

5. The iteration is terminated if $\|\boldsymbol{E}_h^{m+1,k+1} - \boldsymbol{E}_h^{m+1,k}\|/\|\boldsymbol{E}_h^m\| < e_{\text{tol}}$, where e_{tol} is the tolerance of the iteration. Otherwise update index $k = k + 1$ and return to Step 2.

fully implicit method proposed in [32], the reference implicit ECC scheme employs subcycling for particles crossing the cell edge.

It can be seen from (4.1) that the computation requires a nonlinear iteration. In practice, the convergence of the Picard iteration is observed around 2 iterations by choosing $N_s \leq 1$. Due to (3.18), one gets

$$\frac{\rho_h^{m+1,k} - \rho_h^m}{\triangle t} + \nabla_h \cdot \boldsymbol{J}_h^{m+\frac{1}{2},k} = 0, \tag{4.4}$$

where $\rho_h^{m+1,k} = \sum_p \omega_p S_2(x_i - X_p^{m+1,k}) S_2(y_j - Y_p^{m+1,k}) S_2(z_k - Z_p^{m+1,k})$. Thus the charge conservation is satisfied independent of iteration numbers. From Section 3.2, it can be seen that the energy conservation error is determined by the iteration tolerance. Define a linear operator $\mathcal{A}_h$ as

$$\mathcal{A}_h \begin{bmatrix} \boldsymbol{E}_h \\ \boldsymbol{B}_h \end{bmatrix} = \begin{bmatrix} \frac{\lambda^2}{\triangle t} \boldsymbol{E}_h - \frac{1}{2} \nabla_h \times \boldsymbol{B}_h \\ \frac{1}{2} \nabla_h \times \boldsymbol{E}_h + \frac{1}{\triangle t} \boldsymbol{B}_h \end{bmatrix}. \tag{4.5}$$

The linear system (4.3) can be rewritten as

$$\mathcal{A}_h \begin{bmatrix} \boldsymbol{E}_h^{m+1,k+1} \\ \boldsymbol{B}_h^{m+1,k+1} \end{bmatrix} = \begin{bmatrix} \frac{\lambda^2}{\triangle t} \boldsymbol{E}_h^m - \boldsymbol{J}_h^{m+1/2,k} + \frac{1}{2} \nabla_h \times \boldsymbol{B}_h^{m+1,k} \\ \frac{1}{\triangle t} \boldsymbol{B}_h^m - \frac{1}{2} \nabla_h \times \boldsymbol{E}_h^m \end{bmatrix}. \tag{4.6}$$

It is easy to see that $\mathcal{A}_h$ is invertible and well-conditioned when $\triangle t \ll \lambda$, but ill-conditioned with a fixed time step when $\lambda \to 0$.

4.2 Asymptotic-preserving iterative algorithm

We denote by the implicit APECC scheme the asymptotic-preserving iterative algorithm for (3.1)–(3.6). Define a linear operator $\mathcal{M}^{m+1/2}$ such that

$$\mathcal{M}^{m+1/2}(\boldsymbol{E}_h) := \sum_{p=1}^{N_p} \sum_{s=0}^{N_s} \omega_p \boldsymbol{E}_p^{m_s} \cdot \sum_{l=0}^{L_p^{m_s}} \boldsymbol{S}^{m_s,l+1/2}(\boldsymbol{x}_h - \boldsymbol{X}_p) \frac{\tau_{pl}^{m_s}}{\triangle t V_o}, \tag{4.7}$$

where $\boldsymbol{E}_p^{m_s}$ is an averaged electric field along the substep of the p-th particle, defined by

$$\boldsymbol{E}_p^{m_s} = \sum_{l=0}^{L_p^{m_s}} \sum_{\nu} \boldsymbol{E}_\nu \cdot \boldsymbol{S}^{m_s,l+1/2}(\boldsymbol{x}_\nu - \boldsymbol{X}_p) \frac{\tau_{pl}^{m_s}}{\triangle t}. \tag{4.8}$$

Changing the order of summation and summing up with respect to ν, we obtain

$$\mathcal{M}^{m+1/2}(\boldsymbol{E}_h) = \sum_{\nu} \boldsymbol{E}_\nu \cdot \sum_p \omega_p \tilde{\tilde{\boldsymbol{S}}}^{m+1/2}(\boldsymbol{x}_\nu, \boldsymbol{x}_h, \boldsymbol{X}_p), \tag{4.9}$$

where

$$\begin{aligned} \tilde{\tilde{\boldsymbol{S}}}^{m+1/2}(\boldsymbol{x}_\nu, \boldsymbol{x}_h, \boldsymbol{X}_p) = \frac{1}{2} \sum_{s=0}^{N_s} \left(\sum_{l=0}^{L_p^{m_s}} \boldsymbol{S}^{m_s,l+1/2}(\boldsymbol{x}_\nu - \boldsymbol{X}_p) \frac{\tau_{pl}^{m_s}}{\triangle t} \right) \left(\sum_{l=0}^{L_p^{m_s}} \boldsymbol{S}^{m_s,l+1/2}(\boldsymbol{x}_h - \boldsymbol{X}_p) \frac{\tau_{pl}^{m_s}}{\triangle t} \right) \\ + \sum_{0 \leq \alpha < \beta \leq N_s} \left(\sum_{l=0}^{L_p^{m_\alpha}} \boldsymbol{S}^{m_\alpha,l+1/2}(\boldsymbol{x}_\nu - \boldsymbol{X}_p) \frac{\tau_{pl}^{m_\alpha}}{\triangle t} \right) \left(\sum_{l=0}^{L_p^{m_\beta}} \boldsymbol{S}^{m_\beta,l+1/2}(\boldsymbol{x}_h - \boldsymbol{X}_p) \frac{\tau_{pl}^{m_\beta}}{\triangle t} \right). \end{aligned}$$

Moreover, define

$$\tilde{\boldsymbol{J}}_h{}^m = \frac{1}{\triangle t V_o} \sum_{p=1}^{N_p} \omega_p \boldsymbol{V}_p^m \cdot \sum_{s=0}^{N_s} \sum_{l=0}^{L_p^{m_s}} \boldsymbol{S}^{m_s,l+1/2}(\boldsymbol{x}_h - \boldsymbol{X}_p)\tau_{pl}^{m_s}, \tag{4.10}$$

$$\tilde{\boldsymbol{J}}_{\times B}^m = \frac{1}{2\triangle t V_o} \sum_{p=1}^{N_p} \omega_p \sum_{s=0}^{N_s} (\boldsymbol{V}_p^{m_s+1/2} \times \boldsymbol{B}_p^{m_s}) \cdot \sum_{l=0}^{L_p^{m_s}} \boldsymbol{S}^{m_s,l+1/2}(\boldsymbol{x}_h - \boldsymbol{X}_p)\tau_{pl}^{m_s}, \tag{4.11}$$

where $\boldsymbol{B}_p^{m_s} = \sum_{l=0}^{L_p^{m_s}} \sum_\nu \boldsymbol{B}_\nu \cdot \boldsymbol{S}^{m_s,l+1/2}(\boldsymbol{x}_\nu - \boldsymbol{X}_p)\tau_{pl}^{m_s}/\triangle t$. We rewrite $\boldsymbol{J}_h^{m+1/2}$ as

$$\boldsymbol{J}_h^{m+1/2} = \tilde{\boldsymbol{J}}_h{}^m + \triangle t \tilde{\boldsymbol{J}}_{\times B}^m + \frac{\triangle t}{2}\mathcal{M}^{m+1/2}(\boldsymbol{E}_h^{m+1}) + \frac{\triangle t}{2}\mathcal{M}^{m+1/2}(\boldsymbol{E}_h^m). \tag{4.12}$$

Changing Step 3 and Step 4 in Algorithm 1, we obtain an implicit APECC scheme in Algorithm 2.

Algorithm 2 An implicit APECC algorithm for the Vlasov-Maxwell equations

---

1. Given $\boldsymbol{E}_h^m$, $\boldsymbol{B}_h^m$, $\boldsymbol{X}_p^m$, $\boldsymbol{V}_p^m$, start with $\boldsymbol{E}_h^{m+1,k=1} = \boldsymbol{E}_h^m$ (k is the iteration index).

2. For $s = 0, 1, \cdots, N_s$, update $\boldsymbol{X}_p^{m_s+1,k}$ and $\boldsymbol{V}_p^{m_s+1,k}$ by (4.1) with $\boldsymbol{X}_p^{m_0} = \boldsymbol{X}_p^m$, $\boldsymbol{V}_p^{m_0} = \boldsymbol{V}_p^m$.

3. Compute the linear operator $\mathcal{M}^{m+1/2,k}$, and $\tilde{\boldsymbol{J}}_h{}^{m,k}$, $\tilde{\boldsymbol{J}}_{\times B}^{m,k}$, then obtain

$$\bar{\bar{\boldsymbol{J}}}_h^{m+1/2,k} = \tilde{\boldsymbol{J}}_h{}^{m,k} + \triangle t \tilde{\boldsymbol{J}}_{\times B}^{m,k} + \frac{\triangle t}{2}\mathcal{M}^{m+1/2,k}(\boldsymbol{E}_h^m). \tag{4.13}$$

4. Obtain the electric filed $\boldsymbol{E}_h^{m+1,k+1}$ and magnetic field $\boldsymbol{B}_h^{m+1,k+1}$ by solving

$$(\frac{\lambda^2}{\triangle t^2}\mathcal{I} + \frac{1}{2}\mathcal{M}^{m+\frac{1}{2},k})\boldsymbol{E}_h^{m+1,k+1} - \frac{1}{2\triangle t}\nabla_h \times (\boldsymbol{B}_h^{m+1,k+1} + \boldsymbol{B}_h^m) = \frac{\lambda^2}{\triangle t^2}\boldsymbol{E}_h^m - \frac{1}{\triangle t}\bar{\bar{\boldsymbol{J}}}_h^{m+\frac{1}{2},k}, \tag{4.14}$$

$$\frac{1}{\triangle t^2}\boldsymbol{B}_h^{m+1,k+1} + \frac{1}{2\triangle t}\nabla_h \times (\boldsymbol{E}_h^{m+1,k+1} + \boldsymbol{E}_h^m) = \frac{1}{\triangle t^2}\boldsymbol{B}_h^m. \tag{4.15}$$

   Here $\mathcal{I}$ is an identity operator.

5. The iteration is terminated if $\|\boldsymbol{E}_h^{m+1,k+1} - \boldsymbol{E}_h^{m+1,k}\|/\|\boldsymbol{E}_h^m\| < e_{\text{tol}}$, where e_{tol} is the tolerance of the iteration. Otherwise update index $k = k+1$ and return to Step 2.

Different from Algorithm 1, the charge conservation is determined by the iteration tolerance, since the current density at the k-th iteration is computed by

$$\boldsymbol{J}_h^{m+1/2,k+1} = \tilde{\boldsymbol{J}}_h{}^{m,k} + \triangle t \tilde{\boldsymbol{J}}_{\times B}^{m,k} + \frac{\triangle t}{2}\mathcal{M}^{m+1/2,k}(\boldsymbol{E}_h^{m+1,k+1}) + \frac{\triangle t}{2}\mathcal{M}^{m+1/2,k}(\boldsymbol{E}_h^m). \tag{4.16}$$

Equation (4.14)–(4.15) equals to

$$\mathcal{A}_h^{m,k}\begin{bmatrix}\boldsymbol{E}_h^{m+1,k+1}\\ \boldsymbol{B}_h^{m+1,k+1}\end{bmatrix} = \begin{bmatrix}\frac{\lambda^2}{\triangle t^2}\boldsymbol{E}_h^m - \frac{1}{\triangle t}\bar{\bar{\boldsymbol{J}}}_h^{m+1/2,k} + \frac{1}{2\triangle t}\nabla_h \times \boldsymbol{B}_h^m\\ \frac{1}{\triangle t^2}\boldsymbol{B}_h^m - \frac{1}{2\triangle t}\nabla_h \times \boldsymbol{E}_h^m\end{bmatrix}, \tag{4.17}$$

where $\mathcal{A}_h^{m,k}$ is defined by

$$\mathcal{A}_h^{m,k}\begin{bmatrix}\boldsymbol{E}_h\\ \boldsymbol{B}_h\end{bmatrix}=\begin{bmatrix}(\frac{\lambda^2}{\triangle t^2}\mathcal{I}+\mathcal{M}^{m+\frac{1}{2},k})\boldsymbol{E}_h-\frac{1}{2\triangle t}\nabla_h\times\boldsymbol{B}_h\\ \frac{1}{2\triangle t}\nabla_h\times\boldsymbol{E}_h+\frac{1}{\triangle t^2}\boldsymbol{B}_h\end{bmatrix}. \tag{4.18}$$

It is noted that $\mathcal{A}_h^{m,k}$ is invertible and well-conditioned when $\lambda\to 0$ if the eigenvalues of $\mathcal{M}^{m+\frac{1}{2},k}$ are independent of λ. In the next section, we will prove that the convergence of the implicit APECC scheme does not depend on λ.

4.3 Implicit APECC and implicit ECC schemes in the electrostatic regime

The electrostatic can be viewed as the reduced Vlasov-Maxwell system by a vanishing magnetic field. The electric field is computed from a scalar potential ϕ. The Vlasov-Poisson system is written as:

$$\partial_t f+\boldsymbol{v}\nabla_{\boldsymbol{x}}f+\boldsymbol{E}\nabla_{\boldsymbol{v}}f=0, \tag{4.19}$$

$$\boldsymbol{E}=-\nabla_{\boldsymbol{x}}\phi,\quad -\lambda^2\nabla_{\boldsymbol{x}}\cdot(\nabla_{\boldsymbol{x}}\phi)=\rho-1. \tag{4.20}$$

Algorithm 3 An implicit APECC algorithm for the Vlasov-Poisson equations

1. Given ϕ_h^m, $\boldsymbol{X}_p^m$, $\boldsymbol{V}_p^m$, start with $\boldsymbol{E}_h^{m+1,k=1}=-\nabla_h\phi_h^m$ (k is the iteration index).
2. Start from $\boldsymbol{X}_p^{m_0}=\boldsymbol{X}_p^m$, $\boldsymbol{V}_p^{m_0}=\boldsymbol{V}_p^m$. For $s=0,1,\cdots,N_s$, update $\boldsymbol{X}_p^{m_{s+1},k}$ and $\boldsymbol{V}_p^{m_{s+1},k}$ by solving

$$\begin{aligned}\boldsymbol{X}_p^{m_{s+1},k}-\boldsymbol{X}_p^{m_s,k}&=\frac{\tau}{2}(\boldsymbol{V}_p^{m_{s+1},k}+\boldsymbol{V}_p^{m_s,k}),\\ \boldsymbol{V}_p^{m_{s+1},k}-\boldsymbol{V}_p^{m_s,k}&=\frac{1}{2}\sum_{l=0}^{L_p^{m_s,k}}\tau_{pj}^{m_s,k}\Big(\boldsymbol{E}_I^{m+1,k}(\boldsymbol{X}_p^{m_{s,l+\frac{1}{2}},k})+\boldsymbol{E}_I^m(\boldsymbol{X}_p^{m_{s,l+\frac{1}{2}},k})\Big).\end{aligned} \tag{4.21}$$

3. Compute the charge density $\bar{\bar{\rho}}_h^{m+1,k}$ in (4.24).
4. The potential filed $\phi_h^{m+1,k+1}$ are obtained by solving (4.23).
5. The iteration is terminated if $\|\phi_h^{m+1,k+1}-\phi_h^{m+1,k}\|/\|\phi_h^m\|<e_{\text{tol}}$, where e_{tol} is the tolerance of the iteration. Otherwise update index $k=k+1$ and return to Step 2.

In fact, Algorithm 2 can also be employed in the Vlasov-Poisson equations by setting magnetic field to zero. From (4.14), we deduce that

$$\nabla_h\cdot((\frac{\lambda^2}{\triangle t^2}\mathcal{I}+\frac{1}{2}\mathcal{M}^{m+1/2,k})\boldsymbol{E}_h^{m+1,k+1})=\nabla_h\cdot(\frac{\lambda^2}{\triangle t^2}\boldsymbol{E}_h^m-\frac{1}{\triangle t}\bar{\bar{\boldsymbol{J}}}_h^{m+\frac{1}{2},k}). \tag{4.22}$$

Let $\phi_h^{m+1,k+1}$ and ϕ_h^m be the potentials related to $\boldsymbol{E}_h^{m+1,k+1}$ and $\boldsymbol{E}_h^m$, respectively. Using $-\nabla_h\cdot\lambda^2(\nabla_h\phi_h^m)=\rho_h^m-1$, it yields

$$-\nabla_h\cdot((\frac{\lambda^2}{\triangle t^2}\mathcal{I}+\frac{1}{2}\mathcal{M}^{m+1/2,k})\nabla_h\phi_h^{m+1,k+1})=\frac{\bar{\bar{\rho}}_h^{m+1,k}-1}{\triangle t^2}, \tag{4.23}$$

where

$$\bar{\bar{\rho}}_h^{m+1,k} = \rho_h^m - \triangle t \nabla_h \cdot \bar{\bar{\boldsymbol{J}}}_h^{m+\frac{1}{2},k}. \tag{4.24}$$

Applying (4.23) and (4.24), an implicit asymptotic-preserving and energy-charge-conserving (APECC) algorithm for the Vlasov-Poisson system is as follows in Algorithm 3.

Similarly, we modify Algorithm 1 to get the implicit energy-charge conservation (ECC) scheme for the Vlasov-Poisson system in Algorithm 4. Both Algorithm 3 and Algorithm 4 have the property

---

Algorithm 4 An implicit ECC algorithm for the Vlasov-poisson equations

---

1. Given ϕ_h^m, $\boldsymbol{X}_p^m$, $\boldsymbol{V}_p^m$, start with $\boldsymbol{E}_h^{m+1,k=1} = -\nabla_h \phi_h^m$ (k is the iteration index).
2. Start from $\boldsymbol{X}_p^{m_0} = \boldsymbol{X}_p^m$, $\boldsymbol{V}_p^{m_0} = \boldsymbol{V}_p^m$. Update $\boldsymbol{X}_p^{m+1,k}$ and $\boldsymbol{V}_p^{m+1,k}$ by solving (4.21) for $s = 0, 1, \cdots, N_s$.
3. Compute the charge density

$$\rho_h^{m+1,k} = \sum_p \frac{\omega_p}{V_o} S_2(x_i - X_p^{m+1,k}) S_2(y_j - Y_p^{m+1,k}) S_2(z_k - Z_p^{m+1,k}). \tag{4.25}$$

4. The potential filed $\phi_h^{m+1,k+1}$ are obtained by solving

$$-\lambda^2 \nabla_h \cdot (\nabla_h \phi^{m+1,k+1}) = \rho_h^{m+1,k} - 1. \tag{4.26}$$

5. The iteration is terminated if $\|\phi_h^{m+1,k+1} - \phi_h^{m+1,k}\| / \|\phi_h^m\| < e_{\text{tol}}$, where e_{tol} is the tolerance of the iteration. Otherwise update index $k = k + 1$ and return to Step 2.

---

of conserving the total energy:

$$\frac{1}{2} \sum_p \omega_p |\boldsymbol{V}_p^{m+1}|^2 + \frac{\lambda^2}{2} \sum_h |\nabla_h \phi_h^{m+1}|^2 V_o = \frac{1}{2} \sum_p \omega_p |\boldsymbol{V}_p^m|^2 + \frac{\lambda^2}{2} \sum_h |\nabla_h \phi_h^m|^2 V_o. \tag{4.27}$$

5 Asymptotic Preserving

In this section, we will show that the iteration is well-posed and that the convergence of the iteration is *independent of* λ. For simplicity of the exposition, we restrict ourselves to a reduced version of the VM equations with one spatial variable, x, and two velocity variables, $\boldsymbol{v} = (v_x, v_y, 0)^\top$. The electric field has a longitudinal component E_x, and a transverse component E_y, i.e. $\boldsymbol{E} = (E_x(x,t), E_y(x,t), 0)$. Finally, the magnetic field is aligned with the z direction and its magnitude is denoted by B_z, i.e. $\boldsymbol{B} = (0, 0, B_z(x,t))$. The reduced VM system is written as

$$\partial_t f + v_x \partial_x f + (E_x + v_y B_z) \partial_{v_x} f + (E_y - v_x B_z) \partial_{v_y} f = 0, \tag{5.1}$$

$$\lambda^2 \frac{\partial E_x}{\partial t} = -J_x, \quad \lambda^2 \frac{\partial E_y}{\partial t} + \frac{\partial B_z}{\partial x} = -J_y, \quad \frac{\partial B_z}{\partial t} + \frac{\partial E_y}{\partial x} = 0, \tag{5.2}$$

where

$$J_x = \int_{-\infty}^{\infty} \int_{-\infty}^{\infty} f(x, v_x, v_y, t) v_x d\, v_x d\, v_y, \quad J_y = \int_{-\infty}^{\infty} \int_{-\infty}^{\infty} f(x, v_x, v_y, t) v_y d\, v_x d\, v_y. \tag{5.3}$$

The Gauss law reads

$$\lambda^2 \partial_x E_x = \rho - 1, \tag{5.4}$$

where $\rho = \int_{\Omega_x} f(x, v, t)\, dv$.

Taking a uniform grid, denoted by C_g the cell $[(g-1/2)\triangle x, (g+1/2)\triangle x]$ with $g \in \mathbb{Z}^+$, $g \le N$. According to Yee's lattice configuration, the different components of the electromagnetic field and of the current densities are

$$\boldsymbol{E}_h = (E_{x,g-1/2}, E_{y,g-1}, 0)^\top, \quad \boldsymbol{B}_h \ = (0, 0, B_{z,g-1/2})^\top, \quad \boldsymbol{J}_h = (J_{x,g-1/2}, J_{y,g-1}, 0)^\top. \tag{5.5}$$

The linear interpolation of $\boldsymbol{E}_h$ and $\boldsymbol{B}_h$ are denoted by $\boldsymbol{E}_I$ and $\boldsymbol{B}_I$. Using the definition of linear interpolation functions and inverse inequality, it yields

$$\|\boldsymbol{E}_I\|_{L^\infty(\Omega_x)} \le \|\boldsymbol{E}_h\|, \quad \|\nabla \boldsymbol{E}_I\|_{L^\infty(\Omega_x)} \le \frac{2}{\triangle x} \|\boldsymbol{E}_h\|. \tag{5.6}$$

For simplicity, we assume $N_s = 0$ and all of the particles cross the cell edge only once. This can be satisfied when the time step is not particularly large. Let X_p^0, $\boldsymbol{V}_p^0$, $\boldsymbol{E}_h^0$, $\boldsymbol{B}_h^0$ denote X_p^m, $\boldsymbol{V}_p^m$, $\boldsymbol{E}_h^m$, $\boldsymbol{B}_h^m$, respectively. We also denote $X_p^{m+1,k}$, $\boldsymbol{V}_p^{m+1,k}$, $\boldsymbol{E}_h^{m+1,k}$, $\boldsymbol{B}_h^{m+1,k}$, $X_p^{m_{0,l+1/2},k}$, $\tau_{pl}^{m_0,k}$ and $L_p^{m_0,k}$ by X_p^k, $\boldsymbol{V}_p^k$, $\boldsymbol{E}_h^k$, $\boldsymbol{B}_h^k$, $X_p^{l+1/2,k}$, τ_{pl}^k and L_p^k, respectively. The iteration starts from $\boldsymbol{E}_h^{k=1} = \boldsymbol{E}_h^0$, and the k-th iteration is rewritten as

$$\begin{cases} X_p^k - X_p^0 &= \frac{\triangle t}{2}(V_{x,p}^k + V_{x,p}^0), \\ \boldsymbol{V}_p^k - \boldsymbol{V}_p^0 &= \sum\limits_{l=0}^{L_p^k} \frac{\tau_{pl}^k}{2}\big(\boldsymbol{E}_I^k(X_p^{l+\frac{1}{2},k}) + \boldsymbol{E}_I^0(X_p^{l+\frac{1}{2},k}) + (\boldsymbol{V}_p^k + \boldsymbol{V}_p^0) \times \boldsymbol{B}_I^0(X_p^{l+\frac{1}{2},k})\big). \end{cases} \tag{5.7}$$

$$\begin{cases} (\frac{\lambda^2}{\triangle t^2}\mathcal{I} + \frac{1}{2}\mathcal{M}^k)\boldsymbol{E}_h^{k+1} - \frac{1}{2\triangle t}\nabla_h \times (\boldsymbol{B}_h^{k+1} + \boldsymbol{B}_h^0) = \frac{\lambda^2}{\triangle t^2}\boldsymbol{E}_h^0 - \frac{1}{\triangle t}\bar{\boldsymbol{J}}_h^{1/2,k}, \\ \frac{1}{\triangle t}\boldsymbol{B}_h^{k+1} + \frac{1}{2}\nabla_h \times (\boldsymbol{E}_h^{k+1} + \boldsymbol{E}_h^0) = \frac{1}{\triangle t}\boldsymbol{B}_h^0. \end{cases} \tag{5.8}$$

Here $\boldsymbol{V}_p^k = (V_{x,p}^k, V_{y,p}^k, 0)^\top$, the operator $\mathcal{M}^k$ is defined by

$$\mathcal{M}^k(\boldsymbol{E}_h) = \sum_{p=1}^{N_p}\sum_{l=0}^{L_p^k} \omega_p \Big(\sum_{l=0}^{L_p^k}\sum_{\nu} \boldsymbol{E}_\nu \cdot \boldsymbol{S}^{l+\frac{1}{2},k}(x_\nu - X_p)\frac{\tau_{pl}^k}{\triangle t}\Big) \cdot \boldsymbol{S}^{l+1/2,k}(x_h - X_p)\frac{\tau_{pl}^k}{2\triangle x \triangle t}, \tag{5.9}$$

where

$$\boldsymbol{S}^{l+1/2,k}(x_h - X_p) = \boldsymbol{i} \otimes \boldsymbol{i} S_1(x_h - X_p^{l+1/2,k}) + \boldsymbol{j} \otimes \boldsymbol{j} S_1(x_h - X_p^{l+1/2,k}) + \boldsymbol{k} \otimes \boldsymbol{k} S_1(x_h - X_p^{l+1/2,k}).$$

By defining

$$\begin{aligned} \tilde{\boldsymbol{J}}_h^{0,k} &= \sum_{p=1}^{N_p}\sum_{l=0}^{L_p^k} \frac{\omega_p \tau_{pl}^k}{\triangle x \triangle t}\boldsymbol{V}_p^0 \cdot \boldsymbol{S}^{l+1/2,k}(x_h - X_p), \\ \tilde{\boldsymbol{J}}_{\times B}^{0,k} &= \sum_{p=1}^{N_p}\sum_{l=0}^{L_p^k} \frac{\omega_p \tau_{pl}^k}{4\triangle x \triangle t}\big((\boldsymbol{V}_p^k + \boldsymbol{V}_p^0) \times \boldsymbol{B}_p^k\big) \cdot \boldsymbol{S}^{l+1/2,k}(x_h - X_p), \end{aligned}$$

with

$$\boldsymbol{B}_p^k = \sum_{l=0}^{L_p^k}\sum_{\nu} \boldsymbol{B}_\nu \cdot \boldsymbol{S}^{l+1/2,k}(x_\nu - X_p)\tau_{pl}^k/\triangle t = \sum_{l=0}^{L_p^k} \boldsymbol{B}_I(X_p^{l+1/2,k})\tau_{pl}^k/\triangle t, \tag{5.10}$$

the current density at the k-th iteration is computed by

$$\boldsymbol{J}_h^{m+\frac{1}{2},k+1} = \left(\tilde{\boldsymbol{J}}_h^{0,k} + \triangle t \tilde{\boldsymbol{J}}_{\times B}^{0,k} + \frac{\triangle t}{2}\mathcal{M}^k(\boldsymbol{E}_h^0)\right) + \frac{\triangle t}{2}\mathcal{M}^k(\boldsymbol{E}_h^{k+1}) = \bar{\bar{\boldsymbol{J}}}_h^{1/2,k} + \frac{\triangle t}{2}\mathcal{M}^k(\boldsymbol{E}_h^{k+1}). \tag{5.11}$$

Assuming X_p^*, $\boldsymbol{V}_p^*$, $\boldsymbol{E}_h^*$ and $\boldsymbol{B}_h^*$ are the solutions to (3.1)–(3.6), one has

$$\begin{cases} X_p^* - X_p^0 &= \frac{\triangle t}{2}(V_{x,p}^* + V_{x,p}^0), \\ \boldsymbol{V}_p^* - \boldsymbol{V}_p^0 &= \sum\limits_{l=0}^{L_p^*} \frac{\tau_{pl}^*}{2}\left(\boldsymbol{E}_I^*(X_p^{l+\frac{1}{2},*}) + \boldsymbol{E}_I^0(X_p^{l+\frac{1}{2},*}) + (\boldsymbol{V}_p^* + \boldsymbol{V}_p^0) \times \boldsymbol{B}_I^0(X_p^{l+\frac{1}{2},*})\right), \end{cases} \tag{5.12}$$

$$\begin{cases} (\frac{\lambda^2}{\triangle t^2}\mathcal{I} + \frac{1}{2}\mathcal{M}^*)\boldsymbol{E}_h^* - \frac{1}{2\triangle t}\nabla_h \times (\boldsymbol{B}_h^* + \boldsymbol{B}_h^0) = \frac{\lambda^2}{\triangle t^2}\boldsymbol{E}_h^0 - \frac{1}{\triangle t}\bar{\bar{\boldsymbol{J}}}_h^{1/2,*}, \\ \frac{1}{\triangle t}\boldsymbol{B}_h^* + \frac{1}{2}\nabla_h \times (\boldsymbol{E}_h^* + \boldsymbol{E}_h^0) = \frac{1}{\triangle t}\boldsymbol{B}_h^0. \end{cases} \tag{5.13}$$

Here the definitions of $\bar{\bar{\boldsymbol{J}}}_h^{1/2,*}$ and $\mathcal{M}^*$ are similar to $\bar{\bar{\boldsymbol{J}}}_h^{1/2,k}$ and $\mathcal{M}^k$, respectively.

Before approaching our theorems, we make some assumptions.

Assumption 5.1. *Firstly, we assume the initial guess for the iteration satisfies* $\left\|\boldsymbol{E}_h^{k=1} - \boldsymbol{E}_h^*\right\| \le r$. *Secondly, we assume that the time step is smaller than the spatial step* $\triangle t = O(\triangle x^{1+\varepsilon})$, *and the particle mesh is smaller than the grid size,* $h_x = O(h_v) = O(\triangle x^{1+\varepsilon})$, *where* $0 < \varepsilon < 1$. *Thirdly, we assume the bounds of electromagnetic fields are independent of* λ *and satisfy*

$$\|\boldsymbol{E}_h^*\| + \left\|\boldsymbol{E}_h^0\right\| \le M_E, \quad \|\boldsymbol{B}_h^*\| + \left\|\boldsymbol{B}_h^0\right\| \le M_B. \tag{5.14}$$

Finally, we assume the charge density tends to unity as λ *goes to zero and is always positive.*

Remark 5.1. The value of r in the first assumption may affect the rate of convergence, but is *independent of* λ. We will prove that the iteration is compressed through mathematical induction. Since the iteration begins with $\boldsymbol{E}_h^{k=1} = \boldsymbol{E}_h^0$, we may have $\left\|\boldsymbol{E}_h^{k=1} - \boldsymbol{E}_h^*\right\| = O(\triangle t)$ if the solution is smooth in time. The second assumption follows from the inverse inequality in the proof below. However, we relax this restriction in our numerical experiments. The third assumption is based on the fully implicit scheme of the original system, but does not depend on the iteration. Although we cannot prove the results analytically, numerical experiments in Fig.11 support this conjecture. From (5.14), it can bee seen that the velocity of the particle is bounded and there exits a constant M_V which is independent of λ such that

$$\left\|\boldsymbol{V}_p^*\right\| + \left\|\boldsymbol{V}_p^0\right\| \le M_V. \tag{5.15}$$

5.1 The eigenvalues of $\mathcal{M}^k$

In this section, we will prove the eigenvalues of $\mathcal{M}^k$ *do not depend on* λ in the view of algebraic expression. Let $\mathbb{S}_x^k = [S_{x,pg}^k] \in \mathbb{R}^{N_p \times N}$ be a matrix corresponding to the shape function, where

$$S_{x,pg}^k := \sum_{l=0}^{L_p^k} S_1(x_{g-1/2} - X_p^{l+1/2,k})\tau_{pl}^k/\triangle t. \tag{5.16}$$

Define $\mathbb{D}_\omega = [d_{pq}] \in \mathbb{R}^{N_p \times N_p}$ the matrix of the particle weight, with $d_{pq} := \delta_{pq}\omega_p$. Here δ_{pq} is the Kronecker delta. The matrix corresponding to the x-axis component of $\mathcal{M}^k$ is defined by

$$\mathbb{M}_x^k = \frac{1}{2\triangle x}(\mathbb{S}_x^k)^\top \mathbb{D}_\omega \mathbb{S}_x^k. \tag{5.17}$$

It is obvious to find that $\mathbb{M}_x^k$ is a symmetric positive semidefinite matrix. Similarly, define

$$\mathbb{M}_y^k = \frac{1}{2\triangle x}(\mathbb{S}_y^k)^\top \mathbb{D}_\omega \mathbb{S}_y^k,$$

with $\mathbb{S}_y^k = [S_{y,pg}^k] \in \mathbb{R}^{N_p\times N}$ and $S_{y,pg}^k = \sum_{l=0}^{L_p^k} S_1(x_g - X_p^{l+\frac{1}{2},k})\tau_{pl}^k/\triangle t$. The matrix corresponding to $\mathcal{M}^k$ is defined by

$$\mathbb{M}^k = \begin{bmatrix} \mathbb{M}_x^k & 0 \\ 0 & \mathbb{M}_y^k \end{bmatrix}. \tag{5.18}$$

Before we show the eigenvalues of $\mathcal{M}^k$, we consider a matrix similar to $\mathbb{M}_x^k$ denoted by $\mathbb{M}_x^{m+\frac{1}{2}}$. Let $t_p^{m,0} = t^m + \frac{\tau_{p0}^*}{2}$, $t_p^{m,1} = t^m + \tau_{p0}^* + \frac{\tau_{p1}^*}{2}$. Define $\mathbb{S}_x^{m+\frac{1}{2}} = [S_{pg}^{m+\frac{1}{2}}] \in \mathbb{R}^{N_p\times N}$, with

$$S_{pg}^{m+\frac{1}{2}} := \sum_{l=0}^{L_p^*} S_1(x_{g-\frac{1}{2}} - X_p(t_p^{m,l}))\frac{\tau_{pl}^*}{\triangle t}, \tag{5.19}$$

where $X_p(t)$ satisfies (2.9). The matrix $\mathbb{M}_x^{m+\frac{1}{2}}$ is defined by $\mathbb{M}_x^{m+\frac{1}{2}} = \frac{1}{2\triangle x}(\mathbb{S}_x^{m+\frac{1}{2}})^\top \mathbb{D}_\omega \mathbb{S}_x^{m+\frac{1}{2}}$.

The characteristic system for the vlasov equation is

$$\frac{\mathrm{d}x}{\mathrm{d}t} = v, \quad \frac{\mathrm{d}\boldsymbol{v}}{\mathrm{d}t} = \boldsymbol{E}(x) + \boldsymbol{v}\times\boldsymbol{B}(x), \quad x(0) = x_0,\ v(0) = v_0. \tag{5.20}$$

We denote the solution $x = x(x_0, \boldsymbol{v}_0, t)$, $\boldsymbol{v} = \boldsymbol{v}(x_0, \boldsymbol{v}_0, t)$. It can be shown that the mapping $(x_0, \boldsymbol{v}_0) \to (x, \boldsymbol{v})$ has Jacobian one and its inverse function is denoted by $x_0 = x_0(x, \boldsymbol{v}, t)$, $\boldsymbol{v}_0 = \boldsymbol{v}_0(x, \boldsymbol{v}, t)$. The mapping given by $(x, \boldsymbol{v}) \to (x_0, \boldsymbol{v}_0)$ also has Jacobian one. It is followed from the vlasov equation that the distribution function is unchanged along the characteristic line (5.20). Changing the variable of integration by (5.20), we obtain

$$\begin{aligned}\int_{\Omega_x} H_I^2 \cdot \rho(x,t)\, dx &= \int_{\Omega_x}\int_{\Omega_v} H_I^2 f(x,v,t)\, dxdv \\ &= \int_{\Omega_{x_0}}\int_{\Omega_{v_0}} \left[H_I^2(x(x_0,\boldsymbol{v}_0,t))\right] f(x_0,v_0,0)\, dv_0 dx_0,\end{aligned} \tag{5.21}$$

where H_I is the linear interpolation of $\vec{H} \in \mathbb{R}^N$.

Lemma 5.1. *Based on the assumptions in Assumption 5.1, if $\triangle x$ is small enough which is independent of λ, there holds*

$$0 < \frac{1}{10}\min_x \rho(x, t^{m+\frac{1}{2}}) \le \mathrm{eig}(\mathbb{M}_x^{m+\frac{1}{2}}) \le \frac{4}{3}\max_x \rho(x, t^{m+\frac{1}{2}}). \tag{5.22}$$

Here $\mathrm{eig}(\mathbb{M}_x^{m+\frac{1}{2}})$ *denotes the eigenvalue of the matrix* $\mathbb{M}_x^{m+\frac{1}{2}}$.

Proof. For any vector $\vec{H} = [H_{\frac{1}{2}}, H_{\frac{3}{2}}, \cdots, H_{N-\frac{1}{2}}]^\top$, we denote H_I the corresponding linear interpolation function. Since H_I is not smooth, we build a smooth approximation to H_I denoted by H_η through the mollifier [20, Appendix C] such that

$$H_\eta = H_I, \quad \text{in } \Omega_x \backslash \cup_g \Omega_{g,\eta}, \tag{5.23}$$

where $\Omega_{g,\eta} = [x_{g-\frac{1}{2}} - \eta, x_{g-\frac{1}{2}} + \eta]$ and $\eta = O(\triangle x)$. According to the properties of mollifiers [20, Theorem 7, Appendix C], we have

$$\left\|H_\eta^2 - H_I^2\right\|_{L^\infty(\Omega_{g,\eta})} \lesssim H_{g,\max}^2 \triangle x, \tag{5.24}$$

$$\left\|(\partial_x^\alpha H_\eta)^2\right\|_{L^\infty(\Omega_{g,\eta})} \approx \left\|\partial_x^\alpha (H_\eta^2)\right\|_{L^\infty(\Omega_{g,\eta})} \lesssim \frac{H_{g,\max}^2}{\triangle x^\alpha}, \quad \alpha = 1, 2, \tag{5.25}$$

where $H_{g,\max}^2 = \max\{H_{g-\frac{3}{2}}^2, H_{g-\frac{1}{2}}^2, H_{g+\frac{1}{2}}^2\}$. Using (5.21), (5.24)-(5.25) and applying the numerical integration scheme, it yields

$$\begin{aligned}
&\int_{\Omega_x} H_I^2 \cdot \rho(x,t)\, dx = \int_{\Omega_{x_0}} \int_{\Omega_{v_0}} \left[H_\eta^2(x(x_0, \boldsymbol{v}_0, t))\right] f(x_0, v_0, 0)\, dv_0 dx_0 + O(\sum_g H_{g-\frac{1}{2}}^2 \triangle x^2) \\
=& \sum_{p=1}^{N_p} \left[H_\eta^2(x(X_p(0), V_p(0), t))\right] f(X_p(0), V_p(0), 0) h_x h_v + O(\sum_g H_{g-\frac{1}{2}}^2 \triangle x^2) + O(\frac{\sum_g H_{g-\frac{1}{2}}^2 h_x^3}{\triangle x^2}) \\
=& \sum_{p=1}^{N_p} \omega_p (H_\eta^2(X_p(t))) + O(\sum_g H_{g-\frac{1}{2}}^2 \triangle x^{1+3\varepsilon}),
\end{aligned}$$

where $X_p(t) = x(X_p(0), V_p(0), t)$, the last term in the second equality comes from the error of numerical integration, and we have used the definition of ω_p, $h_x = O(h_v) = O(\triangle x^{1+\varepsilon})$. By choosing $t = t^{m+\frac{1}{2}}$, using Taylor's expansion and the property of the mollifier (5.24)-(5.25) , we have

$$\begin{aligned}
\int_{\Omega_x} H_I^2 \cdot \rho(x, t^{m+\frac{1}{2}})\, dx &= \sum_{p=1}^{N_p} \omega_p \big(H_\eta^2(X_p(t^{m+\frac{1}{2}}))\big) + O(\sum_g H_{g-\frac{1}{2}}^2 \triangle x^{1+3\varepsilon}) \\
&= \sum_{p=1}^{N_p} \omega_p \big(\sum_{l=0}^{L_p^*} H_I(X_p(t_p^{m,l})) \frac{\tau_{pl}^*}{\triangle t}\big)^2 + O(\sum_g H_{g-\frac{1}{2}}^2 \triangle x^{1+3\varepsilon}).
\end{aligned} \tag{5.26}$$

Through a simple calculation, one gets

$$\frac{1}{3} \min_x \rho(x, t^{m+\frac{1}{2}}) \sum_g H_{g-1/2}^2 \triangle x \leq \int_{\Omega_x} H_I^2 \cdot \rho(x, t^{m+\frac{1}{2}})\, dx \leq 2 \max_x \rho(x, t^{m+\frac{1}{2}}) \sum_g H_{g-\frac{1}{2}}^2 \triangle x. \tag{5.27}$$

According to the definition of $\mathbb{M}_x^{m+\frac{1}{2}}$, it yields

$$\begin{aligned}
\vec{H}^\top \mathbb{M}_x^{m+\frac{1}{2}} \vec{H} =& \sum_{p=1}^{N_p} \frac{\omega_p}{2\triangle x} \big(\sum_{l=0}^{L_p^*} \sum_g H_{g-1/2} \cdot S_1(x_{g-1/2} - X_p(t_p^{m,l})) \frac{\tau_{pl}^*}{\triangle t}\big)^2 \\
=& \sum_{p=1}^{N_p} \frac{\omega_p}{2\triangle x} \big(\sum_{l=0}^{L_p^*} H_I(X_p(t_p^{m,l})) \frac{\tau_{pl}^*}{\triangle t}\big)^2.
\end{aligned} \tag{5.28}$$

Due to (5.26)-(5.28), there holds

$$\begin{aligned}
\mathrm{eig}_{\min}(\mathbb{M}_x^{m+\frac{1}{2}}) =& \min_{\vec{H}} \frac{\vec{H}^\top \mathbb{M}_x^{m+\frac{1}{2}} \vec{H}}{\vec{H}^\top \vec{H}} \geq \min_{\vec{H}} \frac{\sum_p \omega_p \big(\sum_{l=0}^{L_p^*} H_I(X_p(t_p^{m,l})) \frac{\tau_{pl}^*}{\triangle t}\big)^2}{2\triangle x \sum_g H_{g-\frac{1}{2}}^2} + O(\triangle x^{3\varepsilon}) \\
\geq& \frac{1}{10} \min_x \rho(x, t^{m+\frac{1}{2}}),
\end{aligned} \tag{5.29}$$

when $\triangle x$ is small enough such that $\triangle x \lesssim (\frac{\min_x \rho(x,t^{m+\frac{1}{2}})}{15})^{\frac{1}{3\varepsilon}}$. Here we denote by $\mathrm{eig}_{\min}(\mathbb{M}_x^{m+\frac{1}{2}})$ the minimum eigenvalue of $\mathbb{M}_x^{m+\frac{1}{2}}$. The maximum eigenvalue of $\mathbb{M}_x^{m+\frac{1}{2}}$ satisfies

$$\mathrm{eig}_{\max}(\mathbb{M}_x^{m+\frac{1}{2}}) \leq \max_{\vec{H}} \frac{\sum_p \omega_p \big(\sum_{l=0}^{L_p^*} H_I(X_p(t_p^{m,l})) \frac{\tau_{pl}^*}{\triangle t} \big)^2}{2\triangle x \sum_g H_{g-\frac{1}{2}}^2} + O(\triangle x^{3\varepsilon}) \leq \frac{4}{3} \max_x \rho(x, t^{m+\frac{1}{2}}). \tag{5.30}$$

The proof is finished by the assumption that the charge density is always positive. □

Lemma 5.2. *Assume X_p^* is the solution to (5.12), and X_p^k is the solution to (5.7). The assumptions in Assumption 5.1 hold true. For any vector $\vec{H} = [H_{\frac{1}{2}}, H_{\frac{3}{2}}, \cdots, H_{N-\frac{1}{2}}]^\top \in \mathbb{R}^N$, let H_I denote the corresponding linear interpolation function. Define*

$$H_p^* = \sum_{l=0}^{L_p^*} H_I(X_p^{l+\frac{1}{2},*}) \frac{\tau_{pl}^*}{\triangle t}, \quad H_p^k = \sum_{l=0}^{L_p^k} H_I(X_p^{l+\frac{1}{2},k}) \frac{\tau_{pl}^k}{\triangle t}. \tag{5.31}$$

There holds

$$\big| H_p^* - H_p^k \big| \leq \frac{5}{\triangle x} \|\vec{H}\|_{l^\infty} |X_p^* - X_p^k|. \tag{5.32}$$

Proof. Since the particle crosses the cell edge only once, there are three cases according to the values of L_p^k and L_p^*. In the following we will prove the estimate case by case.
Case 1: In the first case, one has $L_p^* = L_p^k = 1$. For the p-th particle crossing the cell edge $x_{g-\frac{1}{2}}$ from left to right, using the definition of the shape function, there holds

$$S_1(x_{g-\frac{1}{2}} - X_p^{1/2,*}) \frac{\tau_{p0}^*}{\triangle t} = \frac{\tau_{p0}^*}{\triangle t} - \frac{\big(x_{g-\frac{1}{2}} - X_p^0\big)^2}{2\triangle x(X_p^* - X_p^0)}, \quad S_1(x_{g-\frac{1}{2}} - X_p^{3/2,*}) \frac{\tau_{p1}^*}{\triangle t} = \frac{\tau_{p1}^*}{\triangle t} - \frac{\big(X_p^* - x_{g-\frac{1}{2}}\big)^2}{2\triangle x(X_p^* - X_p^0)},$$

where we have used $\tau_{p0}^*/\triangle t = (x_{g-\frac{1}{2}} - X_p^0)/(X_p^* - X_p^0)$ and $\tau_{p1}^*/\triangle t = (X_p^* - x_{g-\frac{1}{2}})/(X_p^* - X_p^0)$. Let

$$\triangle S_{pg}^0 = \frac{\big(x_{g-\frac{1}{2}} - X_p^0\big)^2}{2\triangle x(X_p^* - X_p^0)} - \frac{\big(x_{g-\frac{1}{2}} - X_p^0\big)^2}{2\triangle x(X_p^k - X_p^0)}, \quad \triangle S_{pg}^1 = \frac{\big(X_p^* - x_{g-\frac{1}{2}}\big)^2}{2\triangle x(X_p^* - X_p^0)} - \frac{\big(X_p^k - x_{g-\frac{1}{2}}\big)^2}{2\triangle x(X_p^k - X_p^0)}.$$

A simple calculation shows

$$\triangle S_{pg}^0 = \frac{\big(x_{g-\frac{1}{2}} - X_p^0\big)^2 (X_p^k - X_p^*)}{2\triangle x(X_p^k - X_p^0)(X_p^* - X_p^0)} \leq \frac{|X_p^k - X_p^*|}{2\triangle x}, \tag{5.33}$$

$$\triangle S_{pg}^1 = \left[\frac{\big(X_p^* - x_{g-\frac{1}{2}}\big)^2}{(X_p^k - X_p^0)(X_p^* - X_p^0)} - \frac{2\big(X_p^* - x_{g-\frac{1}{2}}\big)}{(X_p^k - X_p^0)} - \frac{\big(X_p^k - X_p^*\big)}{(X_p^k - X_p^0)} \right] \cdot \frac{X_p^k - X_p^*}{2\triangle x} \leq \frac{2|X_p^k - X_p^*|}{\triangle x}. \tag{5.34}$$

From the definition of linear interpolation function, one gets

$$H_I(X_p^{1/2,*}) \frac{\tau_{p0}^*}{\triangle t} = (H_{g-3/2} - H_{g-1/2}) \cdot \frac{\big(x_{g-\frac{1}{2}} - X_p^0\big)^2}{2\triangle x(X_p^* - X_p^0)} + H_{g-1/2} \cdot \frac{\tau_{p0}^*}{\triangle t}, \tag{5.35}$$

$$H_I(X_p^{3/2,*}) \frac{\tau_{p1}^*}{\triangle t} = (H_{g+1/2} - H_{g-1/2}) \cdot \frac{\big(X_p^* - x_{g-\frac{1}{2}}\big)^2}{2\triangle x(X_p^* - X_p^0)} + H_{g-1/2} \cdot \frac{\tau_{p1}^*}{\triangle t}. \tag{5.36}$$

It follows from (5.33)–(5.36) that

$$|H_p^* - H_p^k| \le |H_{g-3/2} - H_{g-1/2}| \cdot \triangle S_{pg}^0 + |H_{g+1/2}^* - H_{g-1/2}^*| \cdot \triangle S_{pg}^1 \le \frac{5}{\triangle x}\|\vec{H}\|_{l^\infty}|X_p^k - X_p^*|. \quad (5.37)$$

The result for the particle passing through $x_{g-1/2}$ from right to left is similar, we omit it.

Case 2: In the second case, there holds $L_p^k = L_p^* = 0$. Using mean value theorem and inverse inequality yields

$$\left|H_p^* - H_p^k\right| \le \frac{1}{\triangle x}\|\vec{H}\|_{l^\infty}\left|X_p^* - X_p^k\right|. \quad (5.38)$$

Case 3: In the third case, there holds $L_p^k = 0$, $L_p^* = 1$ (or $L_p^k = 1$, $L_p^* = 0$). Again using the mean value theorem and inverse inequality, there holds

$$\left|H_p^* - H_p^k\right| \le \frac{\tau_{p0}^*}{\triangle t}\left|H_p(X_p^{1/2,*}) - H_p(X_p^{1/2,k})\right| + \frac{\tau_{p1}^*}{\triangle t}\left|H_p(X_p^{3/2,*}) - H_p(X_p^{1/2,k})\right| \le \frac{1}{2\triangle x}\|\vec{H}\|_{l^\infty}\left|X_p^* - X_p^k\right|.$$

The proof is completed by the conclusion from the above three cases.

□

Lemma 5.3. *Assume X_p^*, $\boldsymbol{V}_p^*$ are the solutions to (5.12), X_p^k, $\boldsymbol{V}_p^k$ are the solutions to (5.7), and the assumptions in Lemma 5.2 hold. If $\triangle t$ is small enough but independent of λ, there holds*

$$|X_p^* - X_p^k| \lesssim \triangle t^2 \|\boldsymbol{E}_h^* - \boldsymbol{E}_h^k\|, \quad \|\boldsymbol{V}_p^* - \boldsymbol{V}_p^k\| \lesssim \triangle t \|\boldsymbol{E}_h^* - \boldsymbol{E}_h^k\|. \quad (5.39)$$

Proof. For easy notation, let

$$\triangle \boldsymbol{E}_{p1} = \sum_{l=0}^{L_p^*} \boldsymbol{E}_I^*(X_p^{l+1/2,*})\frac{\tau_{pl}^*}{\triangle t} - \sum_{l=0}^{L_p^k} \boldsymbol{E}_I^k(X_p^{l+1/2,k})\frac{\tau_{pl}^k}{\triangle t},$$

$$\triangle \boldsymbol{E}_{p2} = \sum_{l=0}^{L_p^*} \boldsymbol{E}_I^0(X_p^{l+1/2,*})\frac{\tau_{pl}^*}{\triangle t} - \sum_{l=0}^{L_p^k} \boldsymbol{E}_I^0(X_p^{l+1/2,k})\frac{\tau_{pl}^k}{\triangle t}.$$

The estimate for $\triangle \boldsymbol{E}_p = \triangle \boldsymbol{E}_{p1} + \triangle \boldsymbol{E}_{p2}$ is from Lemma 5.2 and the triangle inequality, that is

$$\left\|\triangle \boldsymbol{E}_p\right\| \le \left\|\triangle \boldsymbol{E}_{p1}\right\| + \left\|\triangle \boldsymbol{E}_{p2}\right\| \le \left\|\boldsymbol{E}_h^* - \boldsymbol{E}_h^k\right\| + \frac{5}{\triangle x} M_E \left|X_p^* - X_p^k\right| \quad (5.40)$$

Let $\triangle \boldsymbol{B}_p = \sum_{l=0}^{L_p^*} \boldsymbol{B}_I^0(X_p^{l+1/2,*})\frac{\tau_{pl}^*}{\triangle t} - \sum_{l=0}^{L_p^k} \boldsymbol{B}_I^0(X_p^{l+1/2,k})\frac{\tau_{pl}^k}{\triangle t}$. Using Lemma 5.2 again, one gets

$$\left\|\triangle \boldsymbol{B}_p\right\| \le \frac{5}{\triangle x}\left\|\boldsymbol{B}_h^0\right\|\left|X_p^* - X_p^k\right|. \quad (5.41)$$

According to (5.7) and (5.12), we have

$$\begin{aligned} \triangle \tilde{\boldsymbol{V}}_p^k &= \frac{\triangle t}{2}\left(\triangle \boldsymbol{E}_p + (\boldsymbol{V}_p^* + \boldsymbol{V}_p^0) \times \triangle \boldsymbol{B}_p\right), \\ \boldsymbol{V}_p^* - \boldsymbol{V}_p^k &= \frac{\triangle \tilde{\boldsymbol{V}}_p^k + \frac{\triangle t}{2}\triangle \tilde{\boldsymbol{V}}_p^k \times \boldsymbol{B}_I^0(X_p^{m+1/2,k})}{1 + \frac{\triangle t^2}{4}(B_p^{0,k})^2}, \end{aligned} \quad (5.42)$$

where $B_p^{0,k} = \left|\sum_{l=0}^{L_p^k} B_{Iz}^0(X_p^{l+1/2,k})\frac{\tau_{pl}^k}{\triangle t}\right|$. From (5.40) and (5.41), one gets

$$\left\|\triangle \tilde{\boldsymbol{V}}_p^k\right\| \le \frac{\triangle t}{2}\left\|\boldsymbol{E}_h^* - \boldsymbol{E}_h^k\right\| + \frac{5(M_E + M_V M_B)\triangle t}{2\triangle x}\left|X_p^* - X_p^k\right|.$$

Due to (5.42), there holds

$$\|\boldsymbol{V}_p^* - \boldsymbol{V}_p^k\| \leq \left(1 + \frac{\triangle t}{2}\|\boldsymbol{B}_h^0\|\right)\|\triangle \tilde{\boldsymbol{V}}_p^k\| \leq \frac{C_{v1}\triangle t}{\triangle x}|X_p^* - X_p^k| + C_{v2}\triangle t\|\boldsymbol{E}_h^* - \boldsymbol{E}_h^k\|, \tag{5.43}$$

where $C_{v1} = (\frac{5}{2} + \frac{5}{4}\|\boldsymbol{B}_h^0\|\triangle t)(M_E + M_V M_B)$ and $C_{v2} = \frac{1}{2} + \frac{\triangle t}{4}\|\boldsymbol{B}_h^0\| = \frac{1}{2} + O(\triangle t)$. Since $X_p^* - X_p^k = \frac{\triangle t}{2}(V_{x,p}^* - V_{x,p}^k)$, it is easy to find

$$\left|X_p^* - X_p^k\right| \leq C_x \triangle t^2 \left\|\boldsymbol{E}_h^* - \boldsymbol{E}_h^k\right\|, \tag{5.44}$$

where $C_x = \frac{C_{v2}}{2}(1 - \frac{C_{v1}\triangle t^2}{2\triangle x})^{-1} = \frac{1}{4} + O(\triangle t)$. Substituting (5.44) into (5.43), we have

$$\left\|\boldsymbol{V}_p^* - \boldsymbol{V}_p^k\right\| \leq C_v \triangle t \left\|\boldsymbol{E}_h^* - \boldsymbol{E}_h^k\right\|, \tag{5.45}$$

where $C_v = \frac{C_{v1}C_x\triangle t^2}{\triangle x} + C_{v2} = \frac{1}{2} + O(\triangle t)$. $\square$

Remark 5.2. Define $\triangle \boldsymbol{S}_{p,h} = \sum_{l=0}^{L_p^*} S_1(x_h - X_p^{l+1/2,*})\frac{\tau_{pl}^*}{\triangle t} - \sum_{l=0}^{L_p^k} S_1(x_h - X_p^{l+1/2,k})\frac{\tau_{pl}^k}{\triangle t}$. Choosing $\vec{H} = \vec{e}_h$ whose h-th component is unity and the rest are zero, it follows from Lemma 5.2 and 5.3 that

$$|\triangle \boldsymbol{S}_{p,h}| = \left|H_p^* - H_p^k\right| \leq \frac{5C_x\triangle t^2}{\triangle x}\|\boldsymbol{E}_h^* - \boldsymbol{E}_h^k\|. \tag{5.46}$$

Lemma 5.4. *Based on the assumptions in Lemma 5.1, the eigenvalues of $\mathbb{M}^k$ satisfy*

$$\frac{1}{20}\min_x \rho(x, t^{m+\frac{1}{2}}) \leq \mathrm{eig}(\mathbb{M}^k) \leq 2\max_x \rho(x, t^{m+\frac{1}{2}}), \tag{5.47}$$

when $\triangle t$ is small enough but independent of λ.

Proof. From Section 3.2, it is known that the charge conservation is ensured for any order B-splines for the charge density. Therefore, there exists M_ρ independent of k, m and λ such that

$$\rho_{h,i}^k = \sum_{p=1}^{N_p}\omega_p \sum_{l=0}^{L_p^k} S_i(x_h - X_p^{l+\frac{1}{2},k})\tau_{pl}^k/(\triangle t\triangle x) \leq M_\rho, \quad i = 0, 1, 2. \tag{5.48}$$

For any vector $\vec{H}$, applying (5.32), (5.48) and the estimate for $\triangle \boldsymbol{S}_{p,h}$ in (5.46), we have

$$\begin{aligned}
&\left\|(\mathbb{M}_x^* - \mathbb{M}_x^k)\vec{H}\right\|_{l^\infty} \\
=&\max_h\left|\sum_{p=1}^{N_p}\frac{\omega_p}{2\triangle x}H_p^*\cdot\sum_{l=0}^{L_p^*}S_1(x_h - X_p^{l+\frac{1}{2},*})\frac{\tau_{pl}^*}{\triangle t} - \sum_{p=1}^{N_p}\frac{\omega_p}{2\triangle x}H_p^k\cdot\sum_{l=0}^{L_p^k}S_1(x_h - X_p^{l+\frac{1}{2},k})\frac{\tau_{pl}^k}{\triangle t}\right| \\
=&\max_h\left|\sum_{p=1}^{N_p}\frac{\omega_p}{2\triangle x}(H_p^* - H_p^k)\sum_{l=0}^{L_p^*}S_1(x_h - X_p^{l+\frac{1}{2},*})\frac{\tau_{pl}^*}{\triangle t} + \sum_{p=1}^{N_p}\frac{\omega_p}{2\triangle x}H_p^k\triangle \boldsymbol{S}_{p,h}\right| \\
\leq& C_\rho\triangle t\|\vec{H}\|_{l^\infty}\|\boldsymbol{E}_h^* - \boldsymbol{E}_h^k\|,
\end{aligned} \tag{5.49}$$

where $C_\rho = \frac{5C_x M_\rho\triangle t}{\triangle x}$. Following (5.17), we define $\mathbb{M}_x^* = \frac{1}{2\triangle x}(\mathbb{S}_x^*)^\top\mathbb{D}_\omega\mathbb{S}_x^*$, where $\mathbb{S}_x^* = [S_{pg}^*] \in \mathbb{R}^{N_p\times N}$ and $\mathbb{S}_{pg}^* = \sum_{l=0}^{L_p^*} S_1(x_{g-1/2} - X_p^{l+1/2,*})\frac{\tau_{pl}^*}{\triangle t}$. Clearly, $\mathbb{M}_x^*$ is a symmetric matrix. From (5.49), one gets

$$\left|\mathrm{eig}(\mathbb{M}_\mathrm{x}^\mathrm{k} - \mathbb{M}_\mathrm{x}^*)\right| \leq \mathrm{C}_{\rho\mathrm{E}}\triangle\mathrm{t}, \tag{5.50}$$

where $C_{\rho E} = C_\rho r$. Using the same argument as in the proof of (5.49)-(5.50), combining with the boundedness of $\boldsymbol{E}_h^*$, we obtain

$$\left|\mathrm{eig}(\mathbb{M}_{\mathrm{x}}^{\mathrm{m}+\frac{1}{2}} - \mathbb{M}_{\mathrm{x}}^*)\right| \le \mathrm{C_e}\triangle \mathrm{t}, \tag{5.51}$$

where C_e depends on the exact solution and M_E, M_B. Since $\mathbb{M}_x^*$, $\mathbb{M}_x^k$ and $\mathbb{M}_x^{m+\frac{1}{2}}$ are all symmetric matrix, due to (5.50) and (5.51), we have

$$0 < \frac{1}{20}\min_x \rho(x, t^{m+\frac{1}{2}}) \le \frac{1}{2}\mathrm{eig_{min}}(\mathbb{M}_{\mathrm{x}}^{\mathrm{m}+\frac{1}{2}}) \le \mathrm{eig}(\mathbb{M}_{\mathrm{x}}^{\mathrm{k}}) \le \frac{3}{2}\mathrm{eig_{max}}(\mathbb{M}_{\mathrm{x}}^{\mathrm{m}+\frac{1}{2}}) \le 2\max_{\mathrm{x}} \rho(\mathrm{x}, \mathrm{t}^{\mathrm{m}+\frac{1}{2}}),$$

when $\triangle t \le \min\{1, \frac{\mathrm{eig_{min}}(\mathbb{M}_{\mathrm{x}}^{\mathrm{m}+\frac{1}{2}})}{2(C_{\rho E}+C_e)}\}$. The proof is finished by finding a similar estimate for $\mathbb{M}_y^k$. $\square$

Remark 5.3. Comparing with Algorithm 1, the conservation error of the charge in Algorithm 2 depends on the iteration tolerance. In order to estimate the loss of the discrete continue equation, we define

$$e_c^{m+1} = \left\|(\rho_h^{m+1} - \rho_h^m)/\triangle t + \nabla_h \cdot \boldsymbol{J}_h^{m+\frac{1}{2}}\right\|.$$

Assume the iteration stops at $k = k_0$, one gets $\left\|\boldsymbol{E}_h^{m+1,k_0+1} - \boldsymbol{E}_h^{m+1,k_0}\right\|/\left\|\boldsymbol{E}_h^m\right\| \le e_{\mathrm{tol}}$. From section 3.2, it can be seen that

$$(\rho_h^{m+1} - \rho_h^m)/\triangle t + \nabla_h \cdot (\bar{\bar{\boldsymbol{J}}}_h^{m+\frac{1}{2},k_0} + \frac{\triangle t}{2}\mathcal{M}^{m+\frac{1}{2},k_0}(\boldsymbol{E}_h^{m+1,k_0})) = 0. \tag{5.52}$$

Due to Lemma 5.4, there holds

$$e_c^{m+1} \le \frac{\triangle t}{2}\left|\nabla_h \cdot (\mathcal{M}^{m+\frac{1}{2},k_0}(\boldsymbol{E}_h^{m+1,k_0+1} - \boldsymbol{E}_h^{m+1,k_0}))\right| \le \frac{C_c\triangle t}{\triangle x}\max_x \rho(x, t^{m+\frac{1}{2}})e_{\mathrm{tol}}, \tag{5.53}$$

where the constant C_c is independent of m and λ. Therefore, the error of the discrete continuity equation will not accumulate.

5.2 The well-definedness and convergence of the iteration

Since the numerical scheme is fully implicit, it is obvious that the scheme is consistent with the quasi-neutral system (2.6) when $\lambda = 0$. The key is that the convergence of the iteration does not depend on λ. In this section, we will show the well-definedness and convergence of the iteration algorithm are independent of λ.

Theorem 5.1. *If the assumptions in Lemma 5.4 hold, the iteration of (5.7)-(5.8) is well defined even when λ approaches zero.*

Proof. The computation of (5.7) is easy, we refer to [8] for more details. It suffices to prove that (5.8) is well posed after obtaining X_p^k and $\boldsymbol{V}_p^k$. From (5.8), eliminating $\boldsymbol{B}_h^{k+1}$, we get

$$(\frac{\lambda^2}{\triangle t^2}\mathcal{I} + \frac{1}{2}\mathcal{M}^k)\boldsymbol{E}_h^{k+1} + \frac{1}{4}\nabla_h \times (\nabla_h \times \boldsymbol{E}_h^{k+1}) = \frac{1}{\triangle t}\nabla_h \times \boldsymbol{B}_h^0 + \frac{\lambda^2}{\triangle t^2}\boldsymbol{E}_h^0 - \frac{1}{\triangle t}\bar{\bar{\boldsymbol{J}}}_h^{1/2,k} - \frac{1}{4}\nabla_h \times (\nabla_h \times \boldsymbol{E}_h^0). \tag{5.54}$$

Define a linear operator $\mathcal{L}^k$ such that for any $\boldsymbol{E}_h$,

$$\mathcal{L}^k \boldsymbol{E}_h = \frac{1}{2}\mathcal{M}^k \boldsymbol{E}_h + \frac{1}{4}\nabla_h \times (\nabla_h \times \boldsymbol{E}_h). \tag{5.55}$$

Using $\mathcal{L}^k$, we rewrite (5.54) as

$$(\frac{\lambda^2}{\triangle t^2}\mathcal{I}+\mathcal{L}^k)\boldsymbol{E}_h^{k+1}=(\frac{\lambda^2}{\triangle t^2}\mathcal{I}-\mathcal{L}^k)\boldsymbol{E}_h^0+\frac{1}{\triangle t}\nabla_h\times\boldsymbol{B}_h^0-\tilde{\boldsymbol{J}}_{\times B}^{0,k}-\frac{1}{\triangle t}\tilde{\boldsymbol{J}_h}^{0,k}. \tag{5.56}$$

It suffices to prove that $(\frac{\lambda^2}{\triangle t^2}\mathcal{I}+\mathcal{L}^k)$ is invertible.

The matrix corresponding to operator $\mathcal{L}^k$ is defined by

$$\mathbb{L}^k=\begin{bmatrix}\frac{1}{2}\mathbb{M}_x^k & 0\\ 0 & \frac{1}{2}\mathbb{M}_y^k+\frac{1}{4}\mathbb{C}\end{bmatrix}, \tag{5.57}$$

where $\mathbb{C}\vec{E}_y$ corresponds to $\nabla_h\times\nabla_h\times\boldsymbol{E}_h$ and $\mathbb{C}\in\mathbb{R}^{N\times N}$ is a symmetric matrix defined by

$$\mathbb{C}=\frac{1}{\triangle x^2}\begin{bmatrix}2 & -1 & 0 & 0 & \cdots & -1\\ -1 & 2 & -1 & 0 & \cdots & 0\\ 0 & -1 & 2 & -1 & \cdots & 0\\ 0 & 0 & -1 & 2 & \cdots & 0\\ & & & & \cdots & \\ -1 & 0 & 0 & & \cdots & 2\end{bmatrix}. \tag{5.58}$$

It is easy to find $\vec{E}_y^\top\mathbb{C}\vec{E}_y=\sum_h(\nabla_h\times\boldsymbol{E}_h)\cdot(\nabla_h\times\boldsymbol{E}_h)\geq 0$. However, periodic boundary conditions cannot determine $\boldsymbol{E}_h$ uniquely. The proof is finished by finding $\mathrm{eig}(\frac{\lambda^2}{\triangle t^2}\mathbb{I}+\mathbb{L}^k)>\frac{1}{2}\mathrm{eig}(\mathbb{M}^k)>0$, for any $\lambda\geq 0$. □

Theorem 5.2. *If all the assumptions in Theorem 5.1 hold, there exists a constant $\triangle x_0$ which is independent of λ, we have*

$$\lim_{k\to\infty}\boldsymbol{E}_h^k=\boldsymbol{E}_h^*,\quad \lim_{k\to\infty}\boldsymbol{B}_h^k=\boldsymbol{B}_h^*, \tag{5.59}$$

when $\triangle x\leq\triangle x_0$.

Proof. Following (5.54) and (5.56), we obtain a similar formula

$$(\frac{\lambda^2}{\triangle t^2}\mathcal{I}+\mathcal{L}^*)\boldsymbol{E}_h^*=(\frac{\lambda^2}{\triangle t^2}\mathcal{I}-\mathcal{L}^*)\boldsymbol{E}_h^0+\frac{1}{\triangle t}\nabla_h\times\boldsymbol{B}_h^0-\tilde{\boldsymbol{J}}_{\times B}^{0,*}-\frac{1}{\triangle t}\tilde{\boldsymbol{J}_h}^{0,*}, \tag{5.60}$$

where the definitions of $\mathcal{L}^*$, $\tilde{\boldsymbol{J}}_{\times B}^{0,*}$ and $\tilde{\boldsymbol{J}}_h^{0,*}$ are similar to $\mathcal{L}^k$, $\tilde{\boldsymbol{J}}_{\times B}^{0,k}$ and $\tilde{\boldsymbol{J}}_h^{0,k}$. Subtracting (5.54) from (5.60), there holds

$$(\frac{\lambda^2}{\triangle t^2}\mathcal{I}+\mathcal{L}^k)(\boldsymbol{E}_h^*-\boldsymbol{E}_h^{k+1})=-\frac{1}{\triangle t}(\tilde{\boldsymbol{J}_h}^{0,*}-\tilde{\boldsymbol{J}_h}^{0,k})+(\mathcal{L}^k-\mathcal{L}^*)(\boldsymbol{E}_h^*+\boldsymbol{E}_h^0)+(\tilde{\boldsymbol{J}}_{\times B}^{0,k}-\tilde{\boldsymbol{J}}_{\times B}^{0,*}). \tag{5.61}$$

Let $C_J=C_\rho M_V$. Combining with the estimate of $\triangle\boldsymbol{S}_{p,h}$ and (5.48), (5.44), it is clear to see that

$$\|\tilde{\boldsymbol{J}}_h^{0,*}-\tilde{\boldsymbol{J}}_h^{0,k}\|\leq M_V\sum_{p=1}^{N_p}\frac{\omega_p}{\triangle x}|\triangle\boldsymbol{S}_{p,h}|\leq\frac{C_J\triangle t^2}{\triangle x}\|\boldsymbol{E}_h^*-\boldsymbol{E}_h^k\|. \tag{5.62}$$

Since $(\mathcal{L}^k-\mathcal{L}^*)(\boldsymbol{E}_h^*+\boldsymbol{E}_h^0)=\frac{1}{2}(\mathcal{M}^k-\mathcal{M}^*)(\boldsymbol{E}_h^*+\boldsymbol{E}_h^0)$, it is apparent from (5.49) to find

$$\|(\mathcal{L}^*-\mathcal{L}^k)(\boldsymbol{E}_h^*+\boldsymbol{E}_h^0)\|\leq\frac{1}{2}C_\rho M_E\triangle t\|\boldsymbol{E}_h^*-\boldsymbol{E}_h^k\|. \tag{5.63}$$

Similarly, we get

$$\|\triangle \boldsymbol{V}_{\boldsymbol{B}}\| = \|(\boldsymbol{V}_p^* + \boldsymbol{V}_p^0) \times \boldsymbol{B}_p^* - (\boldsymbol{V}_p^k + \boldsymbol{V}_p^0) \times \boldsymbol{B}_p^k\| \leq C_B \triangle t \|\boldsymbol{B}_h^0\| \|\boldsymbol{E}_h^* - \boldsymbol{E}_h^k\|, \tag{5.64}$$

where $C_B = \frac{5C_x \triangle t}{\triangle x} + C_v$. By the estimate of $\triangle \boldsymbol{S}_{p,h}$, (5.48) and (5.64), the same argument gives

$$\begin{aligned} \|\tilde{\boldsymbol{J}}^{0,*}_{\times B} - \tilde{\boldsymbol{J}}^{0,k}_{\times B}\| &= \|\sum_p \frac{\omega_p}{\triangle x} \triangle \boldsymbol{V}_{\boldsymbol{B}} \cdot \sum_{l=0}^{L_p^k} \boldsymbol{S}^{l+\frac{1}{2},k}(x_h - X_p) \frac{\tau_{pl}^k}{\triangle t} + \sum_p \frac{\omega_p}{\triangle x} (\boldsymbol{V}_p^* + \boldsymbol{V}_p^0) \times \boldsymbol{B}_p^{0,*} \cdot \triangle \boldsymbol{S}_{p,h}\| \\ &\leq C_{VB} \|\boldsymbol{B}_h^0\| \triangle t \|\boldsymbol{E}_h^* - \boldsymbol{E}_h^k\|. \end{aligned} \tag{5.65}$$

Here $C_{VB} = C_J + C_B M_\rho$. From (5.62), (5.63) and (5.65), we conclude that the right term of (5.61) denoted by RHS satisfies

$$\text{RHS} \leq (C_J \triangle x^\varepsilon + 1/2 C_\rho M_E \triangle t + C_{VB} M_B \triangle t) \|\boldsymbol{E}_h^* - \boldsymbol{E}_h^k\|. \tag{5.66}$$

From Lemma 5.4, we find

$$\text{eig}_{\min}(\frac{\lambda^2}{\triangle t^2} \mathbb{I} + \mathbb{L}^k) \geq \frac{\lambda^2}{\triangle t^2} + \frac{1}{2} \text{eig}_{\min}(\mathbb{M}^k). \tag{5.67}$$

Combining (5.66) and (5.67), we obtain

$$\|\boldsymbol{E}_h^* - \boldsymbol{E}_h^{k+1}\| \leq 2(\text{eig}_{\min}(\mathbb{M}^k))^{-1} (C_1 \triangle x^\varepsilon + C_2 \triangle t) \|\boldsymbol{E}_h^* - \boldsymbol{E}_h^k\|, \tag{5.68}$$

where $C_1 = C_J$, $C_2 = C_\rho M_E/2 + C_{VB} M_B$. It can be shown that the iteration sequence is compressed when $\triangle x \leq \min\{1, (\frac{\text{eig}_{\min}(\mathbb{M}^k)}{4C_1})^{\frac{1}{\varepsilon}}, (\frac{\text{eig}_{\min}(\mathbb{M}^k)}{4C_2})^{\frac{1}{1+\varepsilon}}\}$, and these parameters depend on M_V, M_E, M_B and r but not λ. Since we have

$$\boldsymbol{B}_h^{k+1} - \boldsymbol{B}_h^* = \frac{\triangle t}{2} \nabla_h \times (\boldsymbol{E}_h^{k+1} - \boldsymbol{E}_h^*),$$

it is easy to see that $\boldsymbol{B}_h^k$ tends to $\boldsymbol{B}_h^*$ as $\boldsymbol{E}_h^k$ goes to $\boldsymbol{E}_h^*$. □

6 Numerical simulations

In this section, we consider two different one-dimensional test problems to demonstrate the accuracy and performance of the present algorithm. We show properties of energy-charge conservation and asymptotic preservation using standard electrostatic and electromagnetic tests. In both cases, the computational domain is characterized by a uniform mesh and periodic boundary conditions. We will see that while the AP-Particle scheme proposed in [15] loses the energy conservation property, the implicit APECC-methodology is able to control the energy loss within the error tolerance, and while the implicit ECC method does not converge (when $\lambda \to 0$), the implicit APECC scheme still provides excellent accuracy.

To test the energy conservation, we define the discrete energy at time t^m as

$$W_E^m = \frac{\lambda^2}{2} \sum_h (\boldsymbol{E}_h^m)^2 \triangle x, \quad W_B^m = \frac{1}{2} \sum_h (\boldsymbol{B}_h^m)^2 \triangle x, \quad W_V^m = \frac{1}{2} \sum_p \omega_p |\boldsymbol{V}_p^m|^2.$$

And the total energy is defined by $W_T^m = W_E^m + W_B^m + W_V^m$. Besides, we denote by $\triangle W_T^m = |W_T^m - W_T^0|/W_T^0$ the total energy error. In the Vlasov-Poisson equations, $\boldsymbol{E}_h^m = -\nabla_h \phi_h^m$.

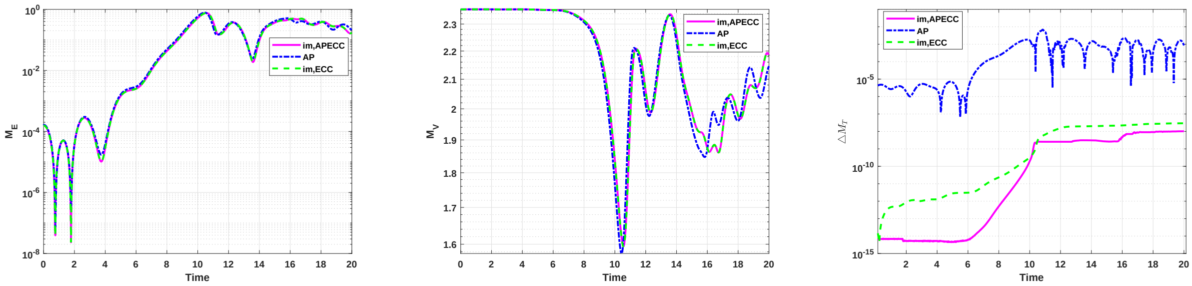

(a) Electric energy as a function of time.
(b) Kinetic energy as a function of time.
(c) Total energy error as a function of time.

Fig. 1: Resolved case of electrostatic tests with $\lambda = 0.5$, calculated by the implicit APECC, the AP and the implicit ECC schemes.

6.1 Electrostatic tests

The system used for this problem is a one-species, one-dimensional, electrostatic model (the magnetic field is disregarded, the ions are motionless uniform backgrounds). The scaled equations are

$$\partial_t f + v\partial_x f + E\partial_v f = 0, \tag{6.1}$$

$$-\partial_x \phi = E, \quad -\lambda^2 \partial_x^2 \phi = \rho - 1. \tag{6.2}$$

The space domain is $[0, 2\pi]$. The initial electron density follows a Maxwellian distribution with a small spatial perturbation

$$f_0(x, v) = (1 + \alpha \cos(x)) \frac{1}{2\sqrt{2\pi}\sigma} e^{-\frac{(v+v_b)^2 + (v-v_b)^2}{2\sigma^2}},$$

where $\alpha = 0.005$, $\sigma = 0.008$ and $v_b = \frac{\sqrt{3}}{2}$. Similar simulations are listed in [9,27,36] .

Two different sets of parameter λ will be considered. All of the tests use $N_p = 10^6$ and $e_{\text{tol}} = 10^{-6}$ in Algorithm 3 and Algorithm 4. In the first case, the scaled Debye length λ is taken equal to 0.5. Fig. 1 shows the simulation results by using the resolved mesh (with $\triangle x = 2\pi/64$, $\triangle t = 0.02$). It can be seen that the error in the total energy calculated with the implicit methods is much lower than that obtained with the AP method. Hence, the kinetic energy calculated by the AP method differs a little from the energy conservation methods for long-time simulations. In terms of the number of iterations per step, the APECC method requires two iterations, while the implicit ECC method generally requires three iterations. Next, we employ large spacial and time steps with $N = 16$, $\triangle t = 1 = 2\lambda$ in the first case. It is shown from Fig. 2 that the implicit APECC method has much better energy conservation properties than the standard implicit ECC method and AP method.

In the second case, we set $\lambda = 5 \cdot 10^{-3}$ to test the asymptotic-preserving property of Algorithm 3. Firstly, we obverse the changes in electric energy, kinetic energy and total energy computed by the implicit APECC, the AP and the implicit ECC method during the time $[0, 1]$ with the resolved mesh ($\triangle x = 2\pi/400$, $\triangle t = 10^{-4}$) in Fig. 3. The errors of total energy are plotted in Fig. 3(c),

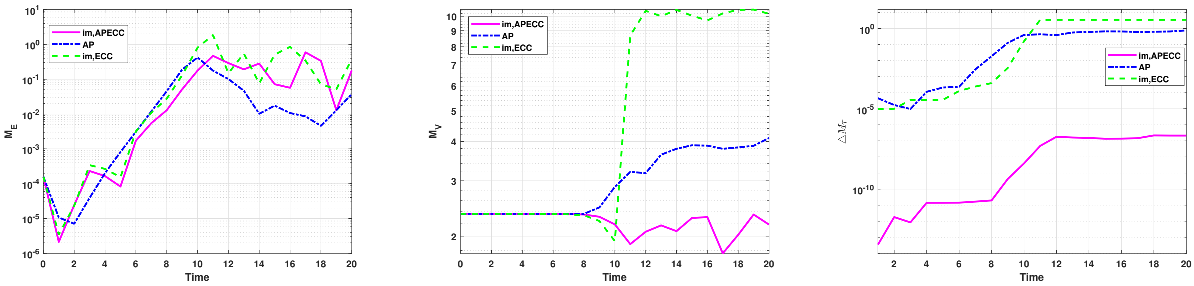

(a) Electric energy as a function of time. (b) Kinetic energy as a function of time. (c) Total energy error as a function of time.

Fig. 2: Under-resolved case of electrostatic tests with $\lambda = 0.5$ calculated by the implicit APECC, the AP and the implicit ECC schemes with $N = 16$, $\triangle t = 2\lambda$.

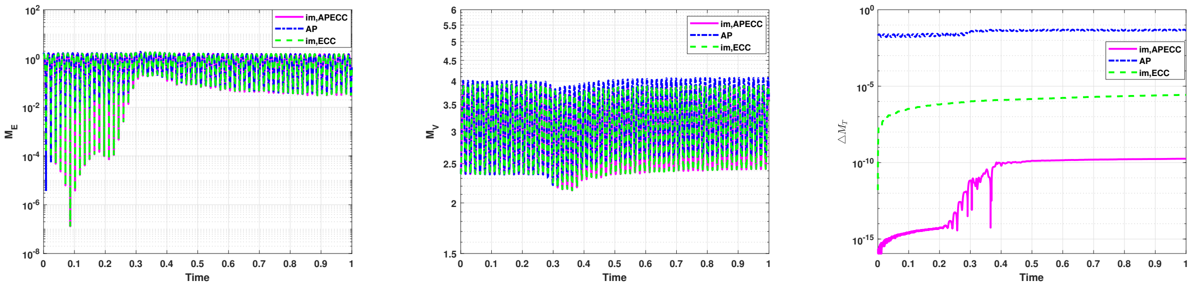

(a) Electric energy as a function of time. (b) Kinetic energy as a function of time. (c) Total energy error as a function of time.

Fig. 3: Resolved case of electrostatic tests with $\lambda = 5 \cdot 10^{-3}$, calculated by the implicit APECC, the AP and the implicit ECC schemes.

which shows that the implicit schemes conserve the energy better than the AP method. We then perform long-time simulations with large spatial sizes and temporal steps. Since the parameter λ controls the smallness of the plasma period with respect to the time scale of the problem, we have $\tau_p \sim \lambda$, where τ_p is the typical period of electron oscillations. Let the simulation stop at $T = 7 \approx 1400\tau_p$. Since the parameter λ is too small, the implicit ECC scheme does not converge within 15 iterations. The outputs of the AP scheme and the implicit APECC scheme are shown in Fig. 4 and Fig. 5. Most strikingly, only the AP scheme simulation with the smaller time step ($\triangle t = 2.5 \cdot 10^{-5}$, $\triangle x = 2\pi/1600$) agrees well with the implicit APECC method, despite the fact that the latter takes a very large special and time step for the simulation ($\triangle x \approx \triangle t = 10\lambda$). For this test, 8 iterations are sufficient to maintain conservation errors at relatively low levels ($\sim 10^{-7}$). Owing to the deterioration of the energy conservation, the AP scheme loses much accuracy.

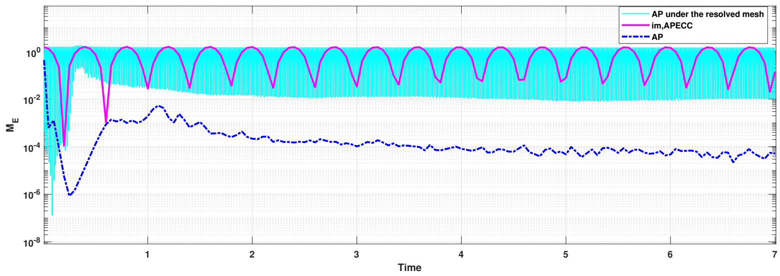

Fig. 4: Under-resolved case of electric energy as a function of time computed by the implicit, APECC and AP method with $\lambda = 5 \cdot 10^{-3}$ and $\triangle x \approx \triangle t = 10\lambda$.

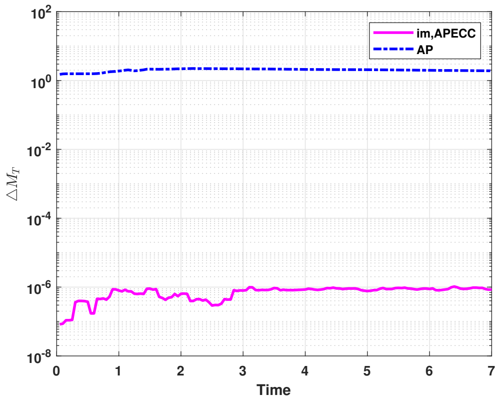

(a) Total energy error as a function of time

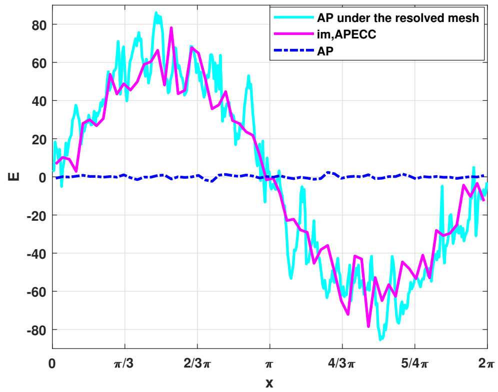

(b) Electric field E at time $T \approx 1400\tau_p$.

Fig. 5: Under-resolved case of electrostatic tests with $\lambda = 5 \cdot 10^{-3}$, calculated by the implicit APECC and the AP schemes with $\triangle x \approx \triangle t = 10\lambda$.

6.2 Electromagnetic tests

In this section, we perform a detailed numerical study of the proposed scheme in the electromagnetic tests. Following [11], the initial conditions for the system (5.1)-(5.3) are given by

$$f(x,, v_x, v_y, 0) = \frac{1}{2\pi\beta} e^{-v_y^2/\beta} (e^{-(v_x - v_b)^2/\beta} + e^{-(v_x+v_b)^2/\beta}), \tag{6.3}$$

$$E_x(x, 0) = E_y(x, 0) = 0, \qquad B_z(x, 0) = b \sin(k_0 x), \tag{6.4}$$

where $\beta = 0.01$, $b = 0.001$, $k_0 = 0.2$ and the space is $[0, 2\pi/k_0]$. We choose $N_p = 8 \cdot 10^6$ and $\mathrm{Tol} = 10^{-6}$ in the following tests. Two different sets of parameter λ will be considered. In the first case, we set $\lambda = 1$. It is a well-known streaming Weibel (SW) instability first analyzed in [34]. The SW instability and its Weibel counterpart have been derived both analytically and numerically in the literature [3–5, 11, 32–34] . In the second test, we choose $\lambda = 5 \cdot 10^{-4}$ to test the asymptotic-preserving behavior.

We first use $\lambda = 1$ with the resolved mesh to test the accuracy. We employ $N = 80$ for the spacial size and $\triangle t = 10^{-1}$ for the time step. It follows from Fig. 6 that the transfer of total energy from kinetic to the fields. We observe that the magnetic and inductive electric fields grow initially at a linear growth rate. All of methods show that saturation occurs at around $t = 80$ in agreement

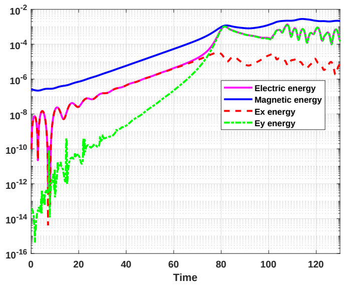

(a) Results of the AP scheme

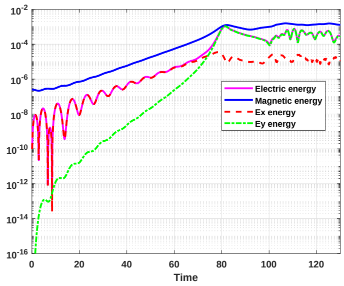

(b) Results of the APECC scheme

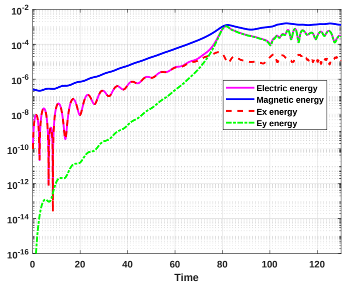

(c) Results of the ECC scheme

Fig. 6: Resolved case of electromagnetic tests with $\lambda = 1$, energy as a function of time calculated by the AP, the implicit APECC and the implicit ECC schemes.

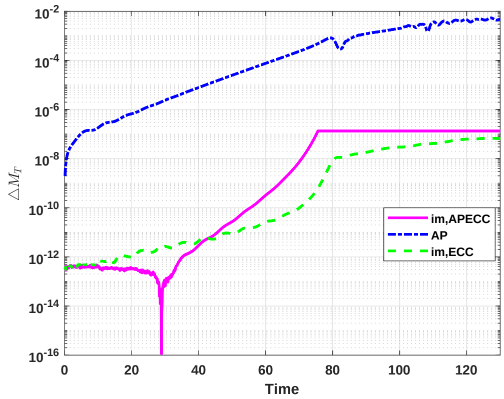

(a) Total energy error as a function of time.

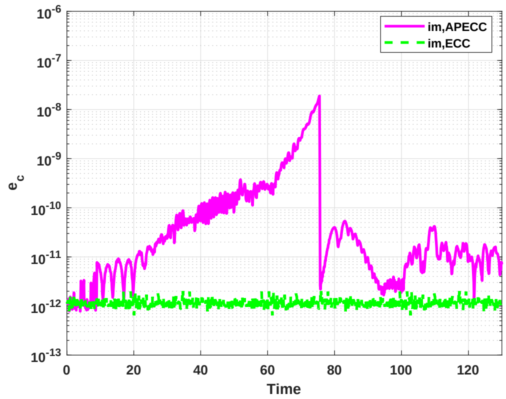

(b) Error of the discrete continue function as a function of time.

Fig. 7: Resolved case of electromagnetic tests with $\lambda = 1$, calculated by the AP, implicit APECC and ECC schemes.

with [11]. Compared with the AP scheme, the implicit methods exhibit additional oscillations due to their use of a second-order time approximation to Maxwell's equations. From Fig. 7(a), the implicit methods have a better behavior on the energy-charge conservation. Although the implicit APECC scheme does not guarantee the continuity equation exactly, it maintains a low level of error from Fig. 7(b).

In the second test, we use a tiny parameter $\lambda = 5 \cdot 10^{-4}$ with large spacial and temporal sizes to test the asymptotic preservation. Similar to the electrostatic tests, the implicit ECC scheme does not work. The reference results are computed by the AP scheme with discretization parameters resolving the Debye length (with $\triangle t = 10^{-5}$, $N = 120$, and $N_p = 4 \cdot 10^7$), whereas the AP scheme and the implicit APECC scheme are now used with large steps (with $\triangle t = 20\lambda$, $N = 32$). We observe from Fig. 8 that the simulation results of the implicit APECC scheme agree more with those with the resolved mesh, no matter the change of electric energy or magnetic energy. Fig. 9 shows the values of the electromagnetic field and density at the final time compared to the reference results. The charge density and magnetic field are in the best agreement with the reference solution.

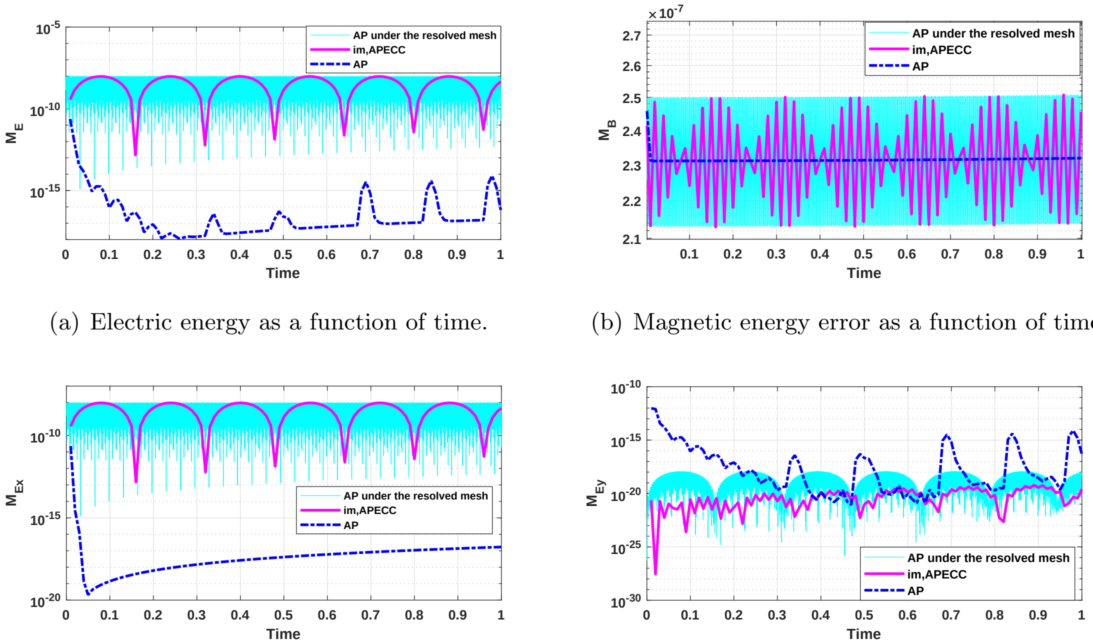

(a) Electric energy as a function of time. (b) Magnetic energy error as a function of time.

(c) Energy of E_x as a function of time. (d) Energy of E_y as a function of time.

Fig. 8: Under-resolved case of Electromagnetic tests with $\lambda = 5 \cdot 10^{-4}$, electromagnetic energy as a function of time calculated by the implicit APECC and the AP schemes with $\triangle t = 20\lambda$, $N = 32$.

The electric fields are in good agreement with the shape, although their values differ from those of the reference results. To compare loss of energy and charge due to the numerical schemes, Fig. 10(a) shows the error of total energy and Fig. 10(b) shows the error of discrete continues equation. Since the AP scheme uses Boris correction to enforce Gauss's law, we only show the results of the implicit APECC scheme in Fig. 10(b). From Fig. 10, we obverse that the implicit APECC scheme conserves both energy and charge. Moreover, three iterations are sufficient for the implicit APECC scheme for either $\lambda = 1$ or $\lambda = 5 \cdot 10^{-4}$.

Finally, we test the behavior of the implicit APECC scheme and (5.6) in Assumption 5.1 when $\lambda \to 0$. Fig. 11 shows the numerical results for the electromagnetic fields after one time step from $t = 0$ with $\triangle t = 20\lambda$, $N = 32$. It can be seen that the numerical solutions converge as λ tends to zero. In addition, this iterative algorithm has a very fast convergence rate and usually converges in three iterations, which is independent of λ.

7 Conclusion

An implicit, Asymptotic-Preserving and energy-charge-conserving Particle-In-Cell method for the Vlasov-Maxwell system in the quasi-neutral limit has been presented. The proposed method has been demonstrated analytically and numerically for its properties of conserving exactly the total energy and charge controlled by a small error tolerance value, and asymptotically preserving near quasineutrality. This implicit method is based on the orbital averaging of particle substeps and decomposition of the current density into an implicit and explicit term.

In this paper, we do not mention the numerical treatment of the boundary conditions, although

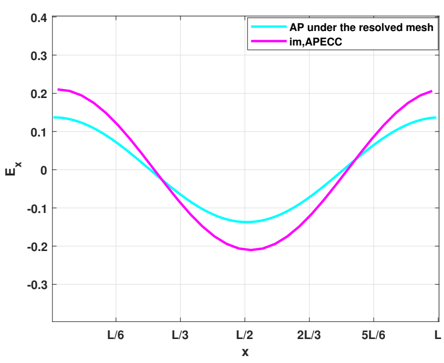

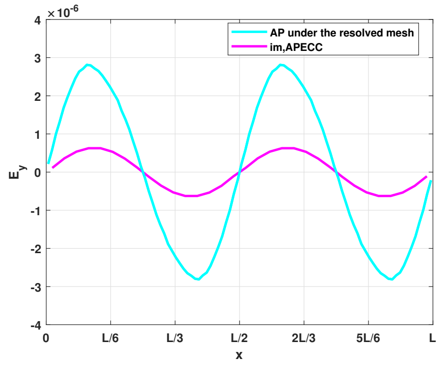

(a) Electric filed E_x at time $T = 1 \approx 2000\tau_p$. (b) Electric filed E_y at time $T = 1 \approx 2000\tau_p$.

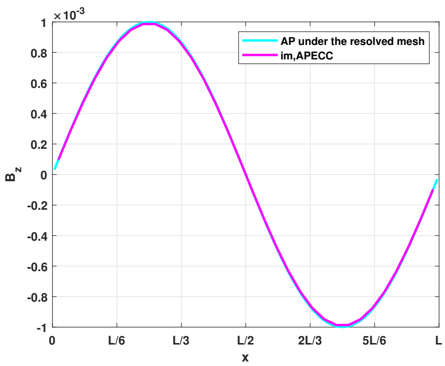

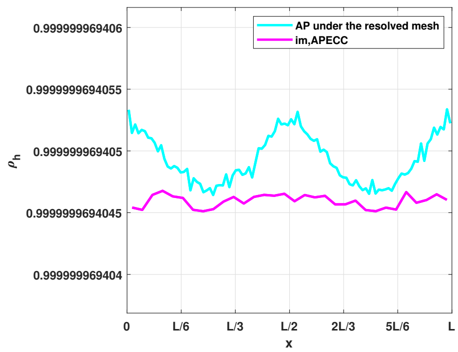

(c) Magnetic filed B_z at time $T = 1 \approx 2000\tau_p$. (d) Charge density ρ_h at time $T = 1 \approx 2000\tau_p$.

Fig. 9: Under-resolved case of Electromagnetic tests with $\lambda = 5 \cdot 10^{-4}$, plots of electromagnetic field and density calculated by the implicit APECC scheme with $\triangle t = 20\lambda$, $N = 32$.

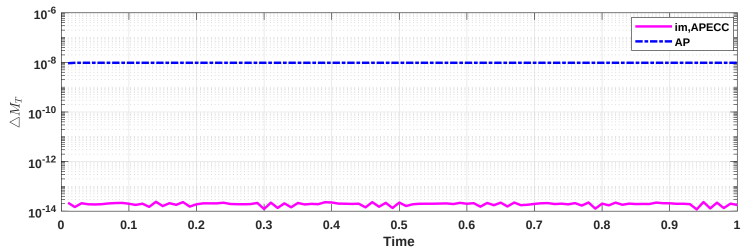

(a) Total energy error as a function of time.

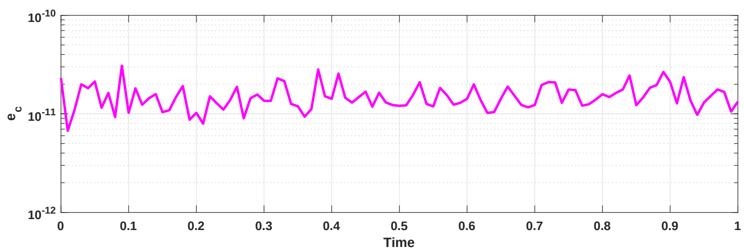

(b) Error of the discrete continue equation as a function of time.

Fig. 10: Under-resolved case of electromagnetic tests with $\lambda = 5 \cdot 10^{-4}$, the error of total energy and continuity equation calculated by the implicit APECC and the AP schemes.

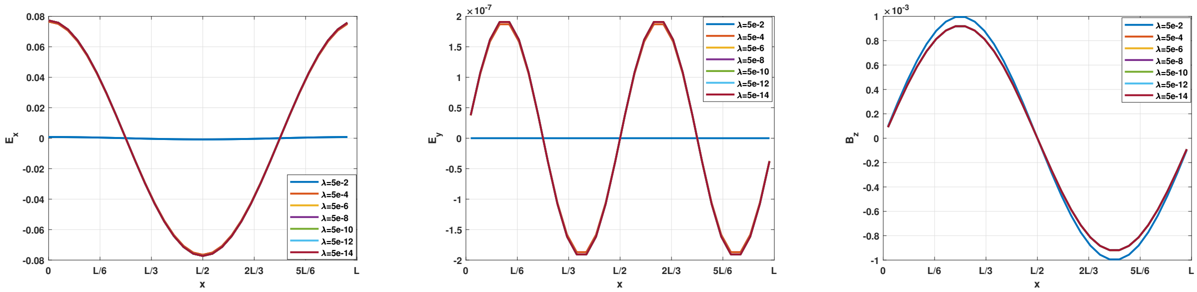

(a) Electric filed E_x (b) Electric filed E_y (c) Magnetic filed B_z

Fig. 11: Under-resolved case of electromagnetic tests calculated by the implicit APECC scheme with $\triangle t = 20\lambda$, $N = 32$ when $\lambda \to 0$.

the method is naturally applicable to periodic boundary conditions. Note that the physical boundary conditions do not affect the energy-charge conservation and asymptotic preservation properties, but they add to the complexity of the numerical implementation. The theorems in this paper are based on Assumption 5.1 and this should be the subject of future work.

Acknowledgments

The research was supported in part by the Strategic Priority Research Program of Chinese Academy of Sciences XDA25010401.

References

[1] C.K. Birdsall and A.B. Langdon. *Plasma physics via computer simulation*. CRC press, 2018.

[2] M. Bostan. Analysis of a particle method for the one-dimensional vlasov-maxwell system. *Methods Partial. Differ. Equ.*, 25(4):757–782, 2009.

[3] F. Califano, N. Attico, F. Pegoraro, G. Bertin, and S.V. Bulanov. Fast formation of magnetic islands in a plasma in the presence of counterstreaming electrons. *Phys. Rev. Lett.*, 86(23):5293–5296, 2001.

[4] F. Califano, F. Pegoraro, and S.V. Bulanov. Impact of kinetic processes on the macroscopic nonlinear evolution of the electromagnetic-beam-plasma instability. *Phys. Rev. Lett.*, 84(16):3602–3605, 2000.

[5] F. Califano, F. Pegoraro, S.V. Bulanov, and A. Mangeney. Kinetic saturation of the weibel instability in a collisionless plasma. *Phys. Rev. E*, 57(6):7048–7059, 1998.

[6] F.F. Chen. *Introduction to plasma physics and controlled fusion*, volume 1. Springer, 1984.

[7] G. Chen and L. Chacón. A multi-dimensional, energy-and charge-conserving, nonlinearly implicit, electromagnetic vlasov–darwin particle-in-cell algorithm. *Comput. Phy. Comm*, 197:73–87, 2015.

[8] G. Chen and L. Chacón. An implicit, conservative and asymptotic-preserving electrostatic particle-in-cell algorithm for arbitrarily magnetized plasmas in uniform magnetic fields. *arXiv preprint arXiv:2205.09187*, 2022.

[9] G. Chen, L. Chacón, and D.C. Barnes. An energy-and charge-conserving, implicit, electrostatic particle-in-cell algorithm. *J. Comput. Phys.*, 230(18):7018–7036, 2011.

[10] G. Chen, L. Chacón, L. Yin, B.J. Albright, D.J. Stark, and R.F. Bird. A semi-implicit, energy- and charge-conserving particle-in-cell algorithm for the relativistic vlasov-maxwell equations. *J. Comput. Phys.*, 407:109228, 2020.

[11] Y. Cheng, I.M. Gamba, F. Li, and P.J. Morrison. Discontinuous galerkin methods for the vlasov–maxwell equations. *SIAM J. Numer. Anal.*, 52(2):1017–1049, 2014.

[12] G-H Cottet and P-A Raviart. Particle methods for the one-dimensional vlasov–poisson equations. *SIAM J. Numer. Anal.*, 21(1):52–76, 1984.

[13] G-H Cottet and P-A Raviart. On particle-in-cell methods for the vlasov-poisson equations. *Transport Theor. Statist. Phys.*, 15(1-2):1–31, 1986.

[14] P. Crispel, P. Degond, and M.H. Vignal. An asymptotic preserving scheme for the two-fluid euler–poisson model in the quasineutral limit. *J. Comput. Phys.*, 223(1):208–234, 2007.

[15] P. Degond, F. Deluzet, and D. Doyen. Asymptotic-preserving particle-in-cell methods for the vlasov–maxwell system in the quasi-neutral limit. *J. Comput. Phys.*, 330:467–492, 2017.

[16] P. Degond, F. Deluzet, L. Navoret, A.B. Sun, and M.H. Vignal. Asymptotic-preserving particle-in-cell method for the vlasov–poisson system near quasineutrality. *J. Comput. Phys.*, 229(16):5630–5652, 2010.

[17] P. Degond, F. Deluzet, and D. Savelief. Numerical approximation of the euler–maxwell model in the quasineutral limit. *J. Comput. Phys.*, 231(4):1917–1946, 2012.

[18] P. Degond, C. Parzani, and M.H. Vignal. A one-dimensional model of plasma expansion. *Math. Comput. Model.*, 38(10):1093–1099, 2003.

[19] P. Degond, C. Parzani, and M.H. Vignal. Plasma expansion in vacuum: modeling the breakdown of quasi neutrality. *SIAM Multiscale Model. Simul.*, 2(1):158–178, 2003.

[20] L.C. Evans. *Partial differential equations.* American Mathematical Society, 2016.

[21] F. Filbet and S. Jin. A class of asymptotic-preserving schemes for kinetic equations and related problems with stiff sources. *J. Comput. Phys.*, 229(20):7625–7648, 2010.

[22] R.N. Franklin and J.R. Ockendon. Asymptotic matching of plasma and sheath in an active low pressure discharge. *J. Plasma Phys.*, 4(2):371–385, 1970.

[23] K. Ganguly and H.D. Victory, Jr. On the convergence of particle methods for multidimensional vlasov–poisson systems. *SIAM J. Numer. Anal.*, 26(2):249–288, 1989.

[24] R. Glassey and J. Schaeffer. Convergence of a particle method for the relativistic vlasov–maxwell system. *SIAM J. Numer. Anal.*, 28(1):1–25, 1991.

[25] F. Golse and L. Saint-Raymond. The vlasov–poisson system with strong magnetic field in quasineutral regime. *Math. Models Methods Appl. Sci.*, 13(05):661–714, 2003.

[26] E. Grenier. Defect measures of the vlasov-poisson system in the quasineutral regime. *Comm. P.D.E.*, 20(7-8):1189–1215, 1995.

[27] A. Ho, I.A.M. Datta, and U. Shumlak. Physics-based-adaptive plasma model for high-fidelity numerical simulations. *Front Phys.*, 6:105, 2018.

[28] L. Ji, Z. Yang, Z. Li, D. Wu, S. Jin, and Z. Xu. An asymptotic-preserving and energy-conserving particle-in-cell method for vlasov-maxwell equations. *arXiv preprint arXiv:2209.08227*, 2022.

[29] S. Jin. Efficient asymptotic-preserving (ap) schemes for some multiscale kinetic equations. *SIAM J. Sci. Comput.*, 21(2):441–454, 1999.

[30] S. Jin. Asymptotic-preserving schemes for multiscale physical problems. *Acta Numerica*, 31:415–489, 2022.

[31] G. Lapenta and S. Markidis. Particle acceleration and energy conservation in particle in cell simulations. *Phys. Plasmas*, 18(7):072101, 2011.

[32] S. Markidis and G. Lapenta. The energy conserving particle-in-cell method. *J. Comput. Phys.*, 230(18):7037–7052, 2011.

[33] L. Palodhi, F. Califano, and F. Pegoraro. Nonlinear kinetic development of the weibel instability and the generation of electrostatic coherent structures. *Plasma Phys. Control. Fusion*, 51(12):125006, 2009.

[34] F. Pegoraro, S.V. Bulanov, F. Califano, and M. Lontano. Nonlinear development of the weibel instability and magnetic field generation in collisionless plasmas. *Phys. Scripta*, 1996(T63):262–265, 1996.

[35] M. Slemrod. The radio-frequency driven plasma sheath: asymptotics and analysis. *SIAM J. Appl. Math.*, 63(5):1737–1763, 2003.

[36] T.H. Stix. *Waves in plasmas.* Springer Science & Business Media, 1992.

[37] A. Taflove, S.C. Hagness, and M. Piket-May. Computational electromagnetics: the finite-difference time-domain method. *The Electrical Engineering Handbook*, 3:629–670, 2005.

[38] H.D. Victory, Jr, G. Tucker, and K. Ganguly. The convergence analysis of fully discretized particle methods for solving vlasov–poisson systems. *SIAM J. Numer. Anal.*, 28(4):955–989, 1991.